

# Transverse Horizontal Coherence and Low-Frequency Array Gain Limits in the Deep Ocean

L. BRUCE PALMER

*Planning Systems Incorporated  
McLean, VA 22102*

and

DENNIS M. DUNDORE, BUDD B. ADAMS, AND JOHN J. MCCOY

*Large Aperture Acoustics Branch  
Acoustics Division*

August 9, 1983



NAVAL RESEARCH LABORATORY  
Washington, D.C.



20. ABSTRACT (Continued)

and hence size, of low-frequency arrays that our present knowledge of the internal structure of the deep ocean will permit.

The special objective of this report is the presentation of an algorithm, the supporting theory of which has previously been published, which has subsequently been supported with a series of experimental investigations of the transverse horizontal coherence properties of the acoustic field following long-range propagation in the deep ocean. From this algorithm the gain of an array can be calculated provided it is restricted to those instances where bottom and surface interaction play a minor part in the overall intensity of the received field.

## CONTENTS

PREFACE .....	iv
INTRODUCTION .....	1
HISTORICAL SUMMARY OF PROPAGATION IN RANDOM MEDIA .....	3
ANALYTIC BACKGROUND .....	6
Wavenumber Representations of Acoustic Fields .....	9
Transverse Horizontal Coherence Model .....	11
Beam Patterns .....	12
Array Signal Gain .....	12
MODEL DESCRIPTION .....	14
Program COHORT .....	15
Signal-Coherence Subroutines .....	15
Subroutine MEDIUM .....	15
Subroutine SPACOH .....	17
Subroutine WAVCOH .....	17
Array-Performance Subroutines .....	18
Subroutine BEAMS .....	18
Subroutine CONVLV .....	19
OPERATING INSTRUCTIONS .....	21
Card-Image Input .....	21
Card-Image Data .....	21
Option Table .....	24
Flowchart .....	24
Sample JSL Commands .....	29
REFERENCES .....	30
APPENDIX — Sample Case .....	32

## PREFACE

This report is a major output of a program in spatial properties of low-frequency acoustic fields in the deep ocean. This project was instituted at the Naval Research Laboratory in 1974 to provide a priori estimates of the capabilities and limitations of large-array construction and performance due to coherence degradation from environmental causes. The project work has emphasized stochastic propagation measures of irregularities in the ocean. This approach has been followed to provide probabilistic predictions of the expected environmental limits to aperture designs.

The order in which contributing elements have been dealt with in this program has been volume effects, bottom effects, and surface effects. The latter two categories are currently under development, while the first category is dealt with in part in this report and is essentially closed at this time. The ordering of the mechanisms and their influence has been guided by the logical separability of volume effects from those that relate to the bottom and/or the surface. Thus, the volume effects treated in the present work provide the outside practical limit on resolution, and hence size, of low-frequency arrays that our present knowledge of the internal structure of the deep ocean will permit. In other words, the resolution limit caused by the forward scattering of the acoustic waves by internal inhomogeneities in the deep ocean can be estimated from the results of the present program. The model provided in this report calculates the horizontal component of this resolution limit.

The special objective of this report is the presentation of an algorithm, whose supporting theory has previously been published, and which has subsequently been supported with a series of experimental investigations of the transverse horizontal coherence properties of the acoustic field following long-range propagation in the deep ocean. From this algorithm the gain of an array can be calculated provided it is restricted to those instances where bottom and surface interaction play a minor part in the overall intensity of the received field. The report includes a detailed discussion of the mutual coherence function which characterizes the kernel of a probabilistic array gain computation, followed by a description of the acoustic field in a wavenumber sense. This is elaborated in considerable detail in the form of a manipulative program designed to handle horizontal line arrays. This development is intended in future works to be enlarged to include the coherence-degrading effects of vertical apertures. In its present form, it provides a framework for the inclusion of the forward-scattering component initially discussed as well as the ability to include further smoothing factors that arise from bottom and surface low-angle forward scattering or diffusion. Such smoothing factors are currently under development. Other program-related reports that extend the dimensionality and range of application of these calculations are listed as Refs. 1 through 4.

# TRANSVERSE HORIZONTAL COHERENCE AND LOW-FREQUENCY-ARRAY GAIN LIMITS IN THE DEEP OCEAN

## INTRODUCTION

A loss in the spatial coherence of an acoustic signal due to random environmental variations places an upper bound on the performance of array systems. The loss of coherence for totally refracted paths results from a stochastic volume scatter, the cause of which can be traced to internal temperature fluctuations. For the range of parameters of interest in low-frequency propagation, these fluctuations can be regarded as a direct result of internal waves. The first-order acoustic-modeling task is to relate the spatial coherence of the received signal to the three-dimensional spectrum of temperature fluctuations characteristic of internal waves.

As a consequence of the high degree of anisotropy of the ocean environment, which has a horizontal quasi-lenticular fine structure, loss in the spatial coherence of a propagating acoustic signal depends strongly on the propagation direction as well as the receiver-pair orientation relative to that fine structure. Thus, over a vertical plane transverse to the direction of propagation, the rate of loss of coherence for horizontally separated receiving positions will be much less than that for vertically separated receiving positions. The rates of loss along lines that form an arbitrary transverse angle with the horizontal will fall between these two extremes. Further, the degree of anisotropy is such that it cannot be readily accommodated by a change of parameters in a single acoustic model. The very structure of the model changes with the direction of the line along which the coherence is to be estimated in the transverse plane. This, along with the presence of a sound-speed field which produces multiple paths, greatly complicates the task of estimating signal coherence over a vertical aperture in comparison to a similar task for a horizontal aperture. Reflecting these differences in the underlying physics, separate models have been developed for horizontal-transverse and for vertical-transverse spatial-coherence estimation.

The model used to estimate transverse horizontal coherence has been designated COHORT and is described extensively in the present report. Models for the estimation of vertically transverse coherence have also been developed — they are termed COVERT and CEM. COVERT estimates the diffusion of a single macroray, and it is most appropriate for acoustic fields that can be approximated by a small number of discrete paths. CEM propagates the mutual coherence function, with scattering, in a range-depth plane, and thus it carries forward an implicit intensity field that is smoothed by multiple low-angle forward scattering. As might be expected, the advantage of propagation of the coherence function is purchased with additional computer capacity and added cost.

The appropriate use of the models described above requires that the distinctive aspects of estimating coherence of an acoustic field be precisely delineated. For example, a conventional propagation model, incorporating a stepping-parabolic-equation algorithm [5], produces complex field points at a given range which may be processed over a depth interval to form the complex-conjugate cross product as a function of vertical point separation. This function, identical in form to the mutual-coherence function, contains only the deterministic part of the acoustic field; its discrete Fourier transform produces the angular distribution of intensity computed over the selected depth interval of the transform. This calculation, in other words, models the beam power-output of an array that has receivers at the

field-point depths and is equal in length to the selected interval. The complex cross-product function from such a calculation generally fluctuates and decreases in value with point separation, i.e., it shows limited "coherence" which is entirely a result of the interfering multipath field. Actually, any set of two or more interfering waves produces "incoherence," so that an experimental measurement or a calculation which accidentally or deliberately includes multipaths will show "loss of coherence." The research in the present program has conceptually and practically separated this multipath, deterministic incoherence from that generated by low-angle scattering to preserve the viewpoint and potential value of concepts like resolution limit, which are most often encountered in optical literature, or other areas where single-path propagation is prominent.

In ocean acoustics, horizontal sound-speed gradients transverse to the propagation direction are seldom, if ever, strong enough to produce horizontal multipaths. Thus, for a horizontal receiving aperture, the single-path concept of resolution limit and transverse horizontal coherence attributable to stochastic mechanisms may be usefully retained. The COHORT model calculates the coherence limit on array signal gain for this precise condition. To reiterate for clarity, the aperture whose performance limit is to be estimated is assumed to be approximately horizontal and transverse to the propagating field whose horizontal coherence is to be calculated. The approximate nature of the orientation is just that required to constrain observable and deterministic multipath-induced coherence effects to some required minimum level. The COVERT model, in a parallel conceptual vein, estimates the single-path resolution limit vertically transverse to the propagating acoustic field along a macroray. Thus, COHORT and COVERT separately estimate the transverse horizontal and vertical components of coherence due to forward scattering, including contributions from all the expected features of an ensemble-averaged picture of ocean acoustic propagation dominantly in the volume. The anisotropy of the ocean, with its tabular or horizontal lenticular structure, plays a major role in the derivation of both models. The principal inhomogeneous component of the ocean, the vertical profile, is also included in both models, *excluding the effects due to multipath*. The Combined Effects Model (CEM) adds the implicit propagation of the transverse multipath structure to the diffusion induced by the anisotropy and modulated by the inhomogeneity. It is thus the most complex model produced to date in the present program.

The COHORT model, described in detail in a later section, is written in a standard form of FORTRAN amenable to conversion to diverse computer systems. It is now in the Texas Instruments Advanced Scientific Computer (ASC) system at NRL and may be accessed from remote terminals. The model is also available through NALCON, a network of interconnected Navy-laboratory computers, for remote operation or total transfer for local operation.

In the remainder of this report, we begin with a short historical summary of propagation in random media. We continue with an analytic background discussion of the coherence function that treats the concepts described above briefly and qualitatively. This is followed by a presentation of the model that evaluates the horizontal signal coherence and a presentation of the wavenumber-space representations, which are particularly useful for coherence estimates. Beam patterns and array signal gain, the desired final result, are covered next. The next section contains a detailed description of the model and its associated subroutines. The COHORT model is a driver program which calls subroutines in accordance with a specific task. The program allows for several optional entry and exit points and for the specification of input parameters at optional levels of detail. This section also serves as a reference which explains the various options in detail. The final main section presents the card-image input data structure, along with a table indicating the cards required by the different options, a flowchart relating input and output data with the subroutines of the model, and a sample set of JSL (Job Specification Language) commands for executing the program on the ASC. A sample execution of program COHORT is given as the appendix.

## HISTORICAL SUMMARY OF PROPAGATION IN RANDOM MEDIA

The modern history of research on the scattering of a radiation field by a randomly fluctuating continuum began during and immediately after World War II. A number of significant studies reported then by Bergmann [6], by Mintzer [7], and by Pekeris [8] were undertaken to explain observations of the effects of temperature fluctuations in the ocean on a propagating acoustic signal. Since the temperature fluctuations are weak and the range of the experiments of interest then was limited, the principal method of analysis was a single-scatter theory, or a Born approximation. Subsequent to these studies there were a number of conceptually and mathematically similar ones motivated by observations of the effects of atmospheric turbulence on a propagating laser-beam signal.

Two monographs, by Chernov [9] and by Tatarski [10], were translated into English and published in 1960 and 1961. These books provided a rather complete survey of the research that had been carried out in the Soviet Union, and they defined what could be termed the state of the art at that time. The research discussed pertained to both acoustic and electromagnetic radiation and emphasized the importance of turbulence as the dynamic process that ultimately gives rise to the scattering. The manuscript by Tatarski was particularly noteworthy for its description of the fluctuating medium and for its reliance on the Kolmogorov spectrum as a correct description of the scattering mechanism. Both monographs were also significant for introducing the Rytov approximation to Western researchers of random-scattering problems. The Rytov approximation, like the Born approximation, is based on perturbation ideas, but the claim of both authors was that the approximation correctly accounted for the multiple-scattering effects necessary for the calculations to be valid for long ranges.

Research into the subject went through a high point in activity, and in controversy, during the sixties, with most of the reported studies treating the scattering of electromagnetic signals in the atmosphere. Much of the controversy centered around two questions: What measures of the statistics of the radiation field are most conveniently determined in physical experiments and most conveniently incorporated in theories? How does one derive theories that properly incorporate multiple scatter effects, as well as the effects of diffraction? A number of studies of the second question were framed in terms of the relative merits of the Born and Rytov approximations.

By the close of the decade of the sixties the controversy on these fundamental questions largely ceased. The central role of the multipoint statistical moments, termed coherence functions in the propagation literature, was recognized by increasing numbers of researchers; techniques had been developed for deriving theories, in the form of differential equations, governing these statistical moments; specific equations had been written for the second- and fourth-order moments, the most crucial moments for discussing experiments; and studies were frequently reported treating the analysis and the solution of these equations in specific applications. A second monograph by Tatarski [11], which appeared in English in 1971, deemphasized the role of the Rytov approximation highlighted in the earlier work. The position espoused in this second monograph appeared to be quite similar to that reached by a growing number of researchers in the United States.

Research in the seventies addressed the need to solve the governing field equations on the second- and fourth-order moments. These efforts included obtaining analytic solutions for idealized experiments and the development of the general numerical algorithms needed to address realistic experiments. In the seventies, also, the specific application appeared to shift away from the scattering of laser beams in the atmosphere to the scattering of acoustic signals in the ocean. While in principle the applications are the same, four factors make an ocean acoustic experiment different in detail. First, the specific statistic of the received signal of interest differs for some acoustic systems. Thus, for example, estimation of the temporal spreading of an acoustic signal received by a single omnidirectional hydrophone is of interest for discussing the performance of communication systems for which the ocean provides the channel. This can be distinguished from the primary motivation for much of the

work on electromagnetic signals carried out in the sixties: the derivation of algorithms for estimating the performance of aperture systems for which the most important measure of the received radiation is of the directional spreading of a signal across the face of an optical lens. This latter application, of course, has its counterpart for signals received by an ocean acoustic array. Second, the dynamic process that gives rise to the fluctuating continuum is different in the ocean acoustic application [12]. Third, the wavelengths of the acoustic signals for the experiments of interest are large (relative to important characteristic lengths) compared to previous, nonacoustic, applications. Fourth, the ocean is an inhomogeneous and a highly anisotropic propagation medium [13-15]. While the second and third of these four factors make the ocean acoustic experiment different from the previous application in degree, the first and fourth can make it different in kind. It is clear that a change in the specific statistic that is of interest would change the nature of the prediction model. It is less clear, although equally true, that the incorporation of inhomogeneity and anisotropy of the medium introduces additional length scales that need to be parameterized in additional nondimensional ratios. Valid prediction modeling will usually require different models for different limiting values of these nondimensional ratios.

Continuing with a synopsis of the advances made in the seventies, a general appreciation of the mathematical identity of the scattering by a randomly inhomogeneous continuum and the quantized motion of a particle in a randomly perturbed potential field [16,17], as well as a duality between a radiative transport theory and the equation governing the two-point coherence function, was achieved during this time span [18-20]. While this appreciation has not greatly altered the general flow of the development of theories, it has introduced new techniques that could prove useful in solving specific problems, e.g., the use of Monte Carlo calculations [21]. Two additional analytic techniques were introduced into the literature of stochastic volume scattering in the seventies. One was the use of the formalism of Feynman path integrals [22]. The other was the formulation of the scattering problem in terms of a modal expansion; the scattering mechanism, in this formulation, results in a coupling via intermodal energy transfer of the normal modes defined for a depth-dependent background medium [23-26]. The motivation for the modal expansion formulation was, clearly, a realization that the ocean environment does define a waveguide, which becomes more obvious with the decreasing frequencies dictated by changing applications.

A number of extended-study programs of the random scattering of acoustic signals by temperature fluctuations were carried out throughout the seventies. Perhaps the most extensive, and certainly the most extensively reported, were the studies of the JASON group; a readable summary of much of their effort has been published in book form [27]. There appear to have been four principal contributions of the JASON studies. First was the emphasis they placed on the need to relate the acoustic event, the stochastic scattering, to the oceanographic events, the presence of internal waves as the controlling dynamic process and of a depth-dependent background sound-speed profile. Second was the importance of combining important characteristic length scales into nondimensional parameters, which can then be used to classify scattering experiments according to separate domains of parameter space. Since the JASON-group research accepts the validity of a model that is rigorously derived for a medium that is both homogeneous and isotropic, only two nondimensional parameters are required to classify all scattering experiments: one is, essentially, the ratio of the experiment range to the range at which diffraction effects become significant, and the other is, essentially, the ratio of the experiment range to the range at which significant acoustic energy (say one-half of the original energy) has been scattered. The third contribution was the introduction of the Feynman path formalism already alluded to above. The fourth contribution was a detailed discussion of a number of reported experiments, principally those reported by Ellinor et al. [28] and by Ewart [29]. Although the basic formalism presented by the JASON group can be applied to a broad spectrum of experiments, it has been applied in detail only to experiments in which the spatial resolution of the signal was not a principal objective. All of the comparisons considered only the statistics of a time series measured at a single point in the acoustic field.

A second extended program of studies was carried out by a less-well-defined group, centered primarily either at New York University or around Tappert (see, for example, Refs. 16-18, 21, 25, and 26). The scope of the program carried out by Tappert et al. was more limited than that of the JASON group; Tappert was essentially interested in the lower order spatial statistics, or in the "aperture problem" that motivated much of the electromagnetic work of the fifties and sixties. Further, this second effort was exclusively either analytical or numerical in nature; no reference was made to any specific series of experiments. The principal contributions were noted earlier in this synopsis: namely, elucidation of the relationship between the ocean acoustics problem and that of the quantized motion of a particle in a perturbed potential field [16,17], the use of Monte Carlo calculations [21], and the formulation of the scattering problem in terms of a modal expansion [25,26].

The third program of studies was carried out by researchers at NRL and by Beran and McCoy, working with NRL. Once again the scope of the study program was limited to estimation of the spatial coherence across a receiving aperture. There were four principal accomplishments. The first was the demonstration that the degree of anisotropy of the scattering mechanism, i.e., that due to internal waves, was such as to necessitate the introduction of a new nondimensional ratio for a complete parameterization of ocean acoustic experiments [13-15]. The scattering models presented in the optical literature of the sixties, or by the JASON group in the seventies, can be shown to be valid as a limit for small values of this anisotropy ratio. This limit can be justified either for propagation in an isotropic medium or for the propagation of high-frequency signals. (For typical experiments, high frequency implies greater than several hundred hertz.)

Second, the initial analysis by the NRL group was concerned with making a number of approximations in order to develop a closed-form expression for estimating the loss of spatial coherence over a billboard array [13,30]. The purpose of this development, which forms the basis of the computational algorithm in the present report, was to provide a realizable calculation which could be programmed for antenna-performance estimates of all types. The many assumptions required were to be physically based and tested with experiments in the ocean. This effort has, to the best of our knowledge, turned out to be successful for horizontal antennas, in that an extensive series of experimental results comparing favorably with the estimates of horizontal coherence produced with the program described here has been assembled and is being published. The initial effort for combined horizontal and vertical apertures showed that multiple parameters were required. Further, it was judged most practical to produce revised, simplified, and improved versions with more limited scope: separate horizontal and vertical antenna models, for example. The first such circumscribed effort addressed the vertical coherence or diffusion for a single path. This effort was carried to conclusion and is available in a calculational package, COVERT, which produces estimates of single path scattering along the selected macroray [1]. This calculation is for those circumstances wherein appeal to the simplification of a discrete field characterization, rays, is warranted. These cases are basically short range, where the multipath effects can be clearly separated from the spreading in the vertical angle estimated by this program.

The third contribution of the NRL group has been the collection of a large body of experimental material relating to the diffusion of an acoustic field in the horizontal regime, as measured for horizontal line arrays, and the comparison of these data with predictions from the closed-form solutions. During the formulation phases of these efforts, many lengthy discussions were held regarding the manner in which component coherences of a multipath structure combine to form the coherence of the total field. For horizontal antennas, however, all the results to date indicate that the incoherent summation of the coherences of multipath components is a feasible simplification. A similar, although lesser, body of experimental material has been assembled and published concerning the distribution of the vertical multipath field.

The fourth stage of the NRL group's analysis has concerned a combined estimation of the coherence effects of refraction and scattering; the model used is called the Combined Effects Model (CEM) [3]. In this calculation the simplifications inherent in the assumption of a single-path field are removed

and the coherence function itself, with an implicit smoothed multipath field, is propagated through the medium. This calculation combines deterministic (multipath) and stochastic (scattering) coherence mechanisms, and it gives the solution to vertical multipath problems that are calculated to ranges which render the discrete-field model of COVERT unacceptable. Whether the discrete-field vertical model or the more complicated vertical model termed CEM is appropriate for a given situation depends upon the objective of the study.

In summary, low-frequency, transverse acoustic dispersion in the deep ocean has been measured and modeled by the NRL group. Transverse horizontal coherence resulting from stochastic volume inhomogeneity has been most intensively studied, and it is the subject of the present prediction-model reported, COHORT. Transverse vertical coherence has been treated in two ways, as described, and will be covered in subsequent reports.

## ANALYTIC BACKGROUND

In the Introduction, several concepts basic to understanding the COHORT program were introduced. In this section, we define these basic concepts and show the strengths and limitations by means of examples.

First, the nature of the oceanic environmental anisotropy and the source-receiver locations clearly defines three distinguishable directions, as illustrated in Fig. 1: the depth direction  $z$ , a horizontal direction determined by the source/receiver locations  $x$ , and a horizontal direction transverse to that determined by the source/receiver locations  $y$ .

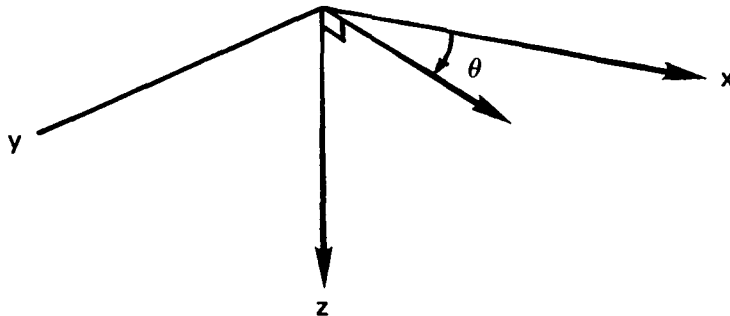


Fig. 1 — Coordinate system

The mathematical measure of the coherence of an acoustic field, which is the fundamental concept of this report, is the ensemble-averaged product of the complex pressure field and its conjugate measured at two points. We write

$$\langle \Gamma(\mathbf{x}_1, \mathbf{x}_2) \rangle = \langle p(\mathbf{x}_1) p^*(\mathbf{x}_2) \rangle, \quad (1)$$

where  $\langle \Gamma(\mathbf{x}_1, \mathbf{x}_2) \rangle$  denotes the coherence function, an asterisk denotes complex conjugation, and the angular brackets denote ensemble averaging.

Our first example is designed to show that, although the coherence function is a stochastic formulation, it is influenced by purely deterministic environmental variations, as well as by random ones. We consider an acoustic field given by two plane waves, each propagating in the  $x$ - $z$  plane, independent of cross range  $y$ , in directions that are inclined to the  $x$  axis by angles  $\phi_1$  and  $\phi_2$ , respectively. (The geometry is shown in Fig. 2.) An experiment in which the received signal can be resolved into arrivals from two different paths of a multipath structure is approximated by this calculation. The complex pressure field for the two plane waves is written

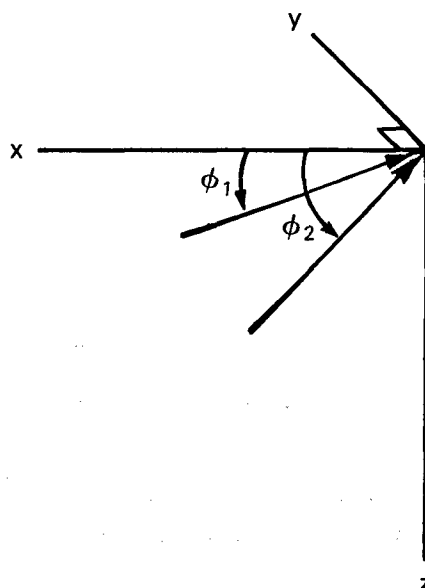


Fig. 2 — Angles of vertical multipath

$$p(\mathbf{x}) = A_1 \exp [ik(\sin \phi_1 z + \cos \phi_1 x)] + A_2 \exp [ik(\sin \phi_2 z + \cos \phi_2 x)], \quad (2)$$

where  $k = 2\pi/\lambda = \omega/c$  is the signal wavenumber,  $c$  being the sound speed in the medium. We form  $\langle \Gamma(z + s/2, z - s/2, x) \rangle$  for two points ( $z \pm s/2$ ), separated by a distance  $s$ , in the same range plane ( $x$ ), for an experiment in which  $A_1$  and  $A_2$  are deterministic (complex) constants. The result can be written as a sum of three terms, i.e.,

$$\langle \Gamma(z + s/2, z - s/2, x) \rangle = \langle \Gamma_1(z, s, x) \rangle + \langle \Gamma_2(z, s, x) \rangle + \langle \Gamma_c(z, s, x) \rangle, \quad (3)$$

where

$$\langle \Gamma_n(z, s, x) \rangle = |A_n|^2 \exp(ik \sin \phi_n s), \quad n = 1, 2, \quad (4a)$$

and

$$\begin{aligned} \langle \Gamma_c(z, s, x) \rangle = 2 \operatorname{Re} \left\{ A_1 A_2^* \exp \{ ik [(\sin \phi_1 - \sin \phi_2)z \right. \\ \left. + (\cos \phi_1 - \cos \phi_2)x] \} \exp \left[ ik \left( \frac{\sin \phi_1 + \sin \phi_2}{2} \right) s \right] \right\}. \quad (4b) \end{aligned}$$

The functions  $\langle \Gamma_1 \rangle$ ,  $\langle \Gamma_2 \rangle$  are the components of the total  $\langle \Gamma \rangle$  that can be associated with the two plane waves existing independently of one another; the function  $\langle \Gamma_c \rangle$  is an interference term.

The "direct coherence" functions ( $\langle \Gamma_1 \rangle$  and  $\langle \Gamma_2 \rangle$ ) oscillate with changes in the separation coordinate ( $s$ ), and these oscillations are a result of the receiver points' lying on a plane that makes an angle with the phase planes of the incoming waves. It is well appreciated that the oscillations of either one of the direct coherence functions are readily removed by introducing a phase shift in the signal received at one of the points, that is, by steering the array to the direction of the incoming signal.

The "interference coherence" function ( $\langle \Gamma_c \rangle$ ) oscillates with changes in either the coordinates ( $x, z$ ) or the separation coordinate ( $s$ ). Further, it is clear from the defining equation that these oscillations cannot be removed by the introduction of a phase shift in the signal received at one of the end points. (It requires an averaging over all possible pair separations of a "filled" array to remove  $\langle \Gamma_c \rangle$ ; see below.) Oscillations in pairwise signal coherence with changes in the positions of the receiver points must always be expected in an experiment in which the received signal arrives from more than one direction. They are a manifestation of a *deterministic* phenomenon, i.e., interference, and are not to

be confused with a "loss" of signal coherence that results from statistical fluctuations in a single-path field.

If one transforms the coherence function with respect to separation ( $s$ ) to obtain a quantity measurable by an array, we find that the interference term  $\langle \Gamma_c \rangle$  gives rise to an expression that oscillates rapidly as a function of the depth. The following statements can be demonstrated:

- For an array sufficiently long to resolve the directions of the two incoming plane waves, the smoothing or averaging of values over the  $z$  coordinate will be sufficient to cancel the oscillations.
- For an array that is insufficiently long to resolve the directions of the two incoming plane waves, the averaging of values will not be sufficient to cancel the oscillations. The nonzero averaged value of the expression in this case is a measure of the interference of the unresolved plane waves.

The main point of the preceding summary was to emphasize that there are a number of "deterministic" factors that affect the pairwise coherence of a narrowband acoustic field as a function of separation distance and that these factors must be considered before any others. Among these deterministic factors are the orientation of the measuring-point pair set to a single propagation direction, as well as the number of components and the angular separation of a multipath structure. We refer to issues of this type as deterministic coherence effects.

Randomness can enter discussions of coherence in two ways. One way is to introduce random perturbations of the parameters that describe the deterministic factors discussed above. These random effects on coherence are usually overridden by the geometric and algebraic aspects of the definition and will not be considered further. A more inclusive aspect of randomness can be introduced by allowing the phase functions of the complex amplitudes ( $A_1$  and  $A_2$ ) to be centered stochastic processes defined over the spatial coordinate. Thus, the expression for  $p(\mathbf{x})$  given by Eq. (2) is replaced by

$$p(\mathbf{x}) = |A_1| \exp [ik(\sin \phi_1 z + \cos \phi_1 x) + i\Phi_1(z, x)] \\ + |A_2| \exp [ik(\sin \phi_2 z + \cos \phi_2 x) + i\Phi_2(z, x)], \quad (5)$$

where  $\Phi_1$  and  $\Phi_2$  are residual stochastic phase functions. We form  $\langle \Gamma(z + s/2, z - s/2, x) \rangle$  as before, and the result can again be written as the sum of three terms, as in Eq. (3), where now

$$\langle \Gamma_n(z, s, x) \rangle = |A_n|^2 \exp(ik \sin \phi_n s) \langle \exp i[\Phi_n(z + s/2, x) - \Phi_n(z - s/2, x)] \rangle \quad (6a)$$

and

$$\langle \Gamma_c(z, s, x) \rangle = |A_1| |A_2| \exp \left[ ik \frac{\sin \phi_1 + \sin \phi_2}{2} \right] \\ \times \left\langle B \exp i \left[ \Phi_1 \left( z + \frac{s}{2} \right) - \Phi_2 \left( z - \frac{s}{2} \right) \right] \right. \\ \left. + B^* \exp -i \left[ \Phi_1 \left( z - \frac{s}{2} \right) - \Phi_2 \left( z + \frac{s}{2} \right) \right] \right\rangle, \quad (6b)$$

where

$$B = \exp \{ ik [(\sin \phi_1 - \sin \phi_2)z + (\cos \phi_1 - \cos \phi_2)x] \}. \quad (6c)$$

To simplify the averaging in Eq. (6) it is necessary to say something of the statistics that govern the  $\Phi_n$ . For illustrative purposes only we assume homogeneous, Gaussian statistics, an assumption that enables us to write

$$\langle \Gamma_n(z, s, x) \rangle = |A_n|^2 \exp(ik \sin \phi_n s) \exp \{-1/2[\sigma_n^2(0) - \sigma_n^2(s)]\}, \quad n = 1, 2, \quad (7a)$$

and

$$\begin{aligned} \langle \Gamma_c(z, s, x) \rangle &= 2 \operatorname{Re} \left\{ |A_1 A_2^*| \exp \{ ik [(\sin \phi_1 - \sin \phi_2)z + (\cos \phi_1 - \cos \phi_2)x] \} \right\} \\ &\times \exp \left[ ik \frac{\sin \phi_1 + \sin \phi_2}{2} s \right] \exp \{ -1/2 [\sigma_1^2(0) + \sigma_2^2(0) - 2\sigma_{12}^2(s)] \}, \end{aligned} \quad (7b)$$

where

$$\sigma_n^2(s) = \langle \Phi_n(0) \Phi_n(s) \rangle, \quad n = 1, 2, \quad (8a)$$

are the correlation functions of the two processes, taken separately, and

$$\sigma_{12}^2(s) = \langle \Phi_1(0) \Phi_2(s) \rangle \quad (8b)$$

is the cross-correlation function of the two processes, taken jointly. For physically realizable systems, the values of the correlation and cross-correlation functions are greatest for zero separation distance and are zero for infinite correlation distance. Also,  $2\sigma_{12}^2(0) < \sigma_1^2(0) + \sigma_2^2(0)$  for physically realizable systems.

Comparing Eqs. (7) to Eqs. (4), we see that the introduction of a randomly varying phase results in an exponential-decay term, with an exponent that depends on the separation. *It is this decay term that describes a coherence loss that is an inherent feature of the statistical nature of the acoustic field and is representative of the stochastic coherence effect of interest in this report.*

### Wavenumber Representations of Acoustic Fields

The acoustic coherence function has been defined by Eq. (1). For the remainder of this report we will consider horizontal coherence only. That is,  $\mathbf{x}_1$  and  $\mathbf{x}_2$  will be restricted to a horizontal line at a depth  $z_0$  and a range  $x$ . This line will define the  $y$ -axis. The acoustic field is assumed to be homogeneous in the (horizontal)  $y$ -direction, in which case  $\langle \Gamma \rangle$  is independent of  $y$ . Therefore, the two-point transverse-horizontal spatial coherence can be written  $\langle \Gamma(s; x, z_0) \rangle$ . In the following, it will be written simply as  $\Gamma(s)$ , with the dependency on  $x$  and  $z_0$  and the ensemble averaging assumed to be understood.

Analogous to the time/frequency Fourier transform pair is the one-dimensional-space/wavenumber transform pair,

$$g(k) = \int_{-\infty}^{+\infty} f(y) e^{-iky} dy \quad (9a)$$

and

$$f(y) = \int_{-\infty}^{+\infty} g(k) e^{+iky} \frac{dk}{2\pi}. \quad (9b)$$

If we define  $\Gamma$  to be the two-point coherence of the signal-only portion of the acoustic field, the *wavenumber spectrum* of the signal (at a fixed frequency  $\omega_0$ ) is

$$S(k) = \int_{-\infty}^{+\infty} \Gamma(s) e^{-iks} ds, \quad -k_0 \leq k \leq k_0, \quad (10)$$

where  $k_0 = \omega_0/c$  and  $c$  is sound speed.

The spectrum  $S(k)$  represents the (horizontal) arrival structure of the signal. This is seen through the relationship

$$k = k_0 \sin \theta. \quad (11)$$

A horizontal receiving line array is assumed to lie along the  $y$ -axis, in which case the angle  $\theta$  is measured relative to broadside of the array (see Fig. 1). For example, a perfectly coherent plane wave of unit amplitude arriving broadside to a linear array has a spatial coherence function (along the array) of

$$\Gamma(s) = 1 \quad (12a)$$

and a wavenumber spectrum of

$$S(k) = S(k_0 \sin \theta) = \delta(0) \cdot 2\pi, \quad (12b)$$

where  $\delta(\cdot)$  is a Dirac-delta function. If we drop the constant  $k_0$  and consider the spectrum as a function of  $\sin \theta$ , the spectrum is zero except when  $\sin \theta = 0$  (i.e.,  $\theta = 0$ , which corresponds to broadside). Figure 3 shows a plot of Eq. (12b). For a perfectly coherent unit-amplitude plane wave arriving from  $30^\circ$  off broadside,

$$\Gamma(s) = e^{ik_0(\sin \pi/6)s} \quad (13a)$$

and

$$S(k) = 2\pi\delta(k - k_0 \sin \pi/6) = 2\pi\delta k_0(\sin \theta - \sin \pi/6). \quad (13b)$$

Figure 4 shows a plot of Eq. (13b).

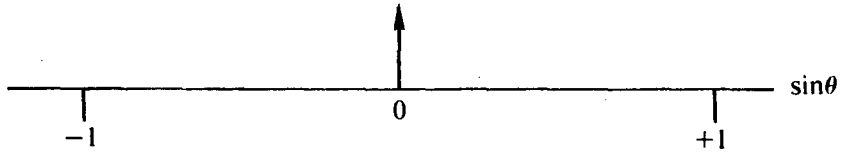


Fig. 3 - Plot of Eq. (12b)

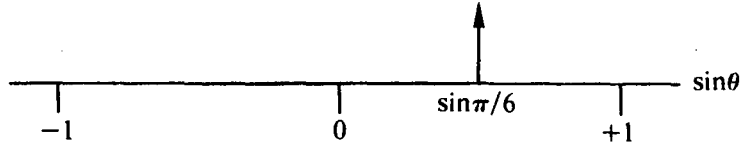


Fig. 4 - Plot of Eq. (13b)

The wavenumber spectrum of a partially coherent signal field is not a delta function, but rather the spectrum is spread in angle, as shown in Fig. 5. Thus, the spectrum  $S(k)$  is seen to represent the (horizontal) arrival structure of the signal as a function of arrival angle  $\theta$ . Furthermore,  $\theta$  varies between  $-\pi/2$  and  $\pi/2$  from broadside (and simultaneously between  $\pi/2$  and  $3\pi/2$ , the front/back ambiguity). Also, for propagating waves (as opposed to, say, electronic noise),

$$S(k) = 0 \text{ for } |k| > k_0, \quad (14a)$$

or equivalently,

$$S(k) = 0 \text{ for } |\sin \theta| > 1, \quad (14b)$$

in which case, the transform pair may be written

$$S(k) = \int_{-\infty}^{+\infty} \Gamma(s) e^{-iks} ds \quad (15a)$$

and

$$\Gamma(s) = \int_{-k_0}^{+k_0} S(k) e^{+iks} \frac{dk}{2\pi}. \quad (15b)$$

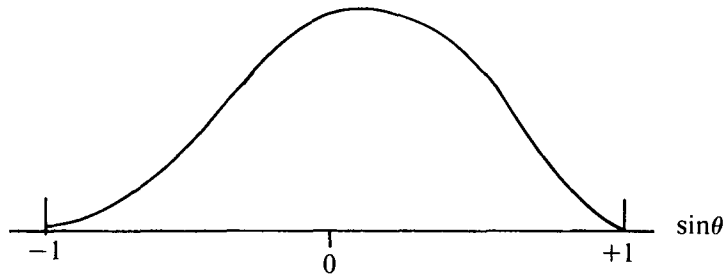


Fig. 5 — Wavenumber spectrum of partially coherent signal field

**Transverse Horizontal Coherence Model**

A formulation for the transverse spatial coherence of an acoustic wavefront in an inhomogeneous and anisotropic ocean has been developed under the auspices of NRL [13-15,19,20,30]. A reduced form estimates horizontal coherence generated by three-dimensional spatial departures of temperature from its mean and, thus, is directly suitable for long, horizontal line arrays. The reduced equation for narrowband signal coherence along a horizontal line transverse to the direction of (entirely-waterborne) propagation from a point source is [14]

$$\Gamma(s) = \Gamma(0) \exp [-Ek_0^{5/2}xs^{3/2}], \tag{16}$$

where

- $x$  = range from the source to the receiver (m),
- $k_0$  = acoustic wavenumber ( $m^{-1}$ ), and
- $s$  = horizontal separation of measurement points (m);

and

$$E = 1.7 \left[ \frac{1}{\bar{c}} \frac{\partial \bar{c}}{\partial T} \right]^2 l_v A_T^2,$$

where

- $\bar{c}$  = average sound speed along path of signal propagation (m/s),
- $T$  = temperature ( $^{\circ}C$ ),
- $\frac{\partial \bar{c}}{\partial T}$  = average derivative of sound speed with respect to temperature along path of signal propagation [(m/s)/ $^{\circ}C$ ],
- $l_v$  = vertical correlation length of temperature fluctuations (m), and
- $A_T^2$  = nominal strength of random temperature field ( $^{\circ}C^2/m$ ).

The above parameters are discussed further in a later section.

The normalized coherence function is defined by

$$\begin{aligned} C(s) &= \Gamma(s)/\Gamma(0) \\ &= \exp [-Ek_0^{5/2}xs^{3/2}]. \end{aligned} \tag{17}$$

The corresponding wavenumber spectrum of the signal is

$$\begin{aligned} S(k) &= \Gamma(0) \int_{-\infty}^{+\infty} \exp (-Ek_0^{5/2}xs^{3/2}) \exp (-iks) ds \\ &= \Gamma(0) \hat{S}(k). \end{aligned} \tag{18}$$

Generally, the spectrum  $\hat{S}(k)$  is determined by numerical integration (transform) because of the 3/2 exponent on the spatial variable.

The range of validity for the transverse coherence model was estimated [30, p. 14] to be 100 Hz to 300 Hz. A recently published set of data, however, shows that it performs well from 100 Hz to 400 Hz. Further, the model estimates were developed as harmonic-wave solutions, i.e., narrowband solutions. However, since dispersion is estimated to be minor, the estimates are expected to be valid for any practical low-frequency signal bandwidth [31, Fig. 5].

### Beam Patterns

Similarly to the wavenumber spectrum of the acoustic field, the response, or array pattern, of a horizontal receiving line array has a wavenumber representation. The array pattern (at fixed frequency  $\omega_0$ ) of a linear array of  $n$  equally spaced, omnidirectional elements is given by

$$B_0(\theta) = \left[ \frac{\sin \left( nk_0 \frac{d}{2} \sin \theta \right)}{n \sin \left( k_0 \frac{d}{2} \sin \theta \right)} \right]^2, \quad (19a)$$

where  $d$  is the element spacing. In wavenumber space,

$$B_0(k) = \left[ \frac{\sin (nkd/2)}{n \sin (kd/2)} \right]^2. \quad (19b)$$

The above equations hold only for equally spaced, perfectly linear (nondeformed) arrays. If the elements are not omnidirectional but have identical beam patterns  $B_g(\theta)$ , the total (or product) array pattern is

$$B_p(k) = B_a(k) B_g(k),$$

where  $B_a(k)$  is the array pattern that would result if all the elements were omnidirectional. A practical example is one in which each identical element of the array consists of a group of omnidirectional hydrophones equally spaced along the array axis. In this case, the element pattern  $B_g(k)$  takes on the form of  $B_0(k)$ , where now  $n$  is the number of omnidirectional hydrophones in each group, and  $d$  is the spacing between individual group hydrophones. Now,

$$B_p(k) = B_a(k) B_0(k).$$

Normally, the outputs from the different hydrophones of a group are summed (e.g., in the array) without time delays. That is, the element or group pattern  $B_g(k)$  is permanently steered to broadside. The receiving pattern is steered by time-delay or phase-rotation of the outputs from the different group elements (i.e., by the steering of the array pattern). For example, if the array pattern is steered in the direction  $k_r = k_0 \sin \theta$ , the product pattern is

$$B_p(k, k_r) = B_a(k - k_r) B_g(k).$$

Note that the major response of this pattern is not necessarily in the direction  $k_r$ .

### Array Signal Gain

For a signal arriving from direction  $\theta_s$  ( $k_s = k_0 \sin \theta_s$ ), with the receiving line array steered to the direction  $\theta_r$ , the power out of the beamformer due to the signal only is given by

$$\begin{aligned} P(k_r, k_s) &= \int_{-k_0}^{+k_0} B_p(k, k_r) S(k - k_s) \frac{dk}{2\pi} \\ &= \Gamma(0) \int B_a(k - k_r) B_g(k) \hat{S}(k - k_s) \frac{dk}{2\pi}. \end{aligned} \quad (21)$$

For a perfectly coherent plane wave,

$$\hat{S}(k) = \delta(k - k_s) \cdot 2\pi$$

and

$$P_0(k_r, k_s) = \Gamma(0) B_a(k_s - k_r) B_g(k_s). \quad (22a)$$

When the array is steered to a signal arriving broadside,

$$P_0(0, 0) = \Gamma(0) B_a(0) B_g(0). \quad (22b)$$

Assuming that the group pattern is well known, it can be normalized such that

$$B_g(0) = 1. \quad (23a)$$

Furthermore, the array pattern can be normalized such that under design conditions (e.g., the array is perfectly linear)

$$B_a(0) = 1 \quad (23b)$$

[otherwise,  $B_a(0) < 1$ ]. In this case,

$$P_0(0, 0) = \Gamma(0). \quad (23c)$$

When the array is steered to a signal arriving from the off-broadside direction  $k_s$ ,

$$\begin{aligned} P_0(k_s, k_s) &= \Gamma(0) B_a(0) B_g(k_s) \\ &= P_0(0, 0) B_g(k_s). \end{aligned} \quad (24)$$

Degradation in array signal gain is defined by

$$L(k_r, k_r) = P(k_r, k_s) / P_0(0, 0), \quad (25)$$

where  $P_0(0, 0)$  is evaluated under design conditions [i.e.,  $B_a(0) = 1$ ,  $P_0(0, 0) = \Gamma(0)$ ]. Therefore, for an arbitrary signal spectrum,

$$L(k_r, k_s) = \int_{-k_0}^{+k_0} B_a(k - k_r) B_g(k) \hat{S}(k - k_s) \frac{dk}{2\pi}. \quad (26)$$

When the array is steered to a perfectly coherent plane wave arriving broadside,

$$L_0(0, 0) = B_a(0). \quad (27)$$

This represents the loss (if any) due to the main-axis response of the array pattern (due, say, to the array becoming nonlinear and  $B_a(0) < 1$ ).

If the array is steered to a perfectly coherent plane wave arriving off broadside,

$$L_0(k_s, k_s) = B_a(0) B_g(k_s), \quad (28)$$

and an additional loss factor of  $B_g(k_r)$  is incurred (due to the group pattern). The loss factor  $B_a(0)$  cannot be corrected for, since it represents a loss due to a deviation from expected conditions [ $B_a(0) = 1$ ]. However, for any steering direction  $k_r$ ,  $B_g(k_r)$  is assumed known and hence can be corrected for by scaling of the product pattern, i.e.,

$$B_p(k, k_r) = B_a(k - k_r) B_g(k) / B_g(k_r), \quad (29a)$$

which ensures that

$$L_0(k_s, k_s) = B_a(0) \quad (29b)$$

when the array is steered to direction  $k_s$ . Accordingly, we rewrite Eq. (26) as

$$L(k_r, k_s) = \frac{1}{B_g(k_r)} \int_{-k_0}^{+k_0} B_a(k - k_r) B_g(k) \hat{S}(k - k_s) \frac{dk}{2\pi}. \quad (30)$$

## MODEL DESCRIPTION

The COHORT model is an implementation of the theory presented in the previous section. Its organization consists of two basic parts. The first part is concerned with computing signal coherence and the second with subsequent array performance. Furthermore, there are three primary options for how the COHORT model may be executed. These options are the following:

- Compute signal coherence only.
- Compute signal coherence and subsequent array performance.
- Input previously calculated signal coherence data and compute array performance.

The flexibility of the model also allows for program entry and termination at different stages within these options and allows input data to be specified in varying degrees of detail.

COHORT consists of a driver program which calls a sequence of subroutines in accordance with a user-defined task. Briefly, these subroutines are as follows:

<b>MEDIUM</b>	Inputs and/or computes environmental parameters needed to evaluate the spatial-coherence model.
<b>SPACOH</b>	Computes, prints, and, optionally, plots and writes the signal spatial-coherence function onto an output file.
<b>WAVCOH</b>	Computes and prints the signal-coherence spectrum of either a computed or an input spatial-coherence function. The spectrum is, optionally, plotted and/or written onto an output file.
<b>BEAMS</b>	Computes and, optionally, plots the group pattern. Reads in or computes and, optionally, plots the array pattern. Reads in the number and amounts of array steers or shifts (i.e., signal-arrival angles) and sets up information for convolution.
<b>CONVLV</b>	For each array pattern shift (signal angle), the product array pattern is computed and convolved with the signal-coherence spectrum to calculate losses in array signal gain, which are printed and, optionally, plotted.

Figure 6 indicates the possible entry and exit points in the above sequence of subroutines.

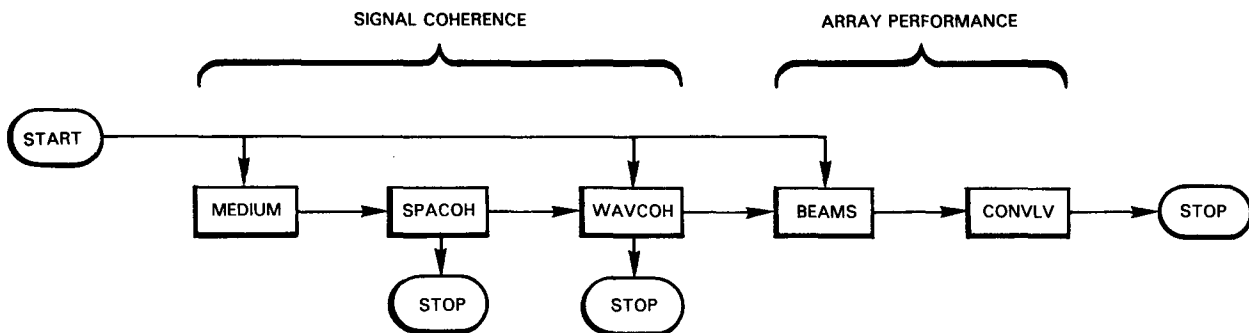


Fig. 6 — Entry and exit options of program COHORT

**Program COHORT**

Program COHORT is a driver program which calls a sequence of subroutines in accordance with task specified by the input variables KBEAM, LCOH, and KCOH. The parameters LCOH and KCOH refer to input and output file unit numbers, whereas KBEAM determines the primary function to be performed. There are three cases definable by the value of KBEAM, as follows:

*Case 1*

KBEAM = 1: The spatial coherence model is evaluated and the coherence spectrum of the signal is computed. Then the resulting losses in array signal gain are determined.

If LCOH > 0, the spatial-coherence function is written onto unit LCOH.

If KCOH > 0, the coherence spectrum is written onto unit KCOH.

*Case 2*

KBEAM = 2: Either the spatial coherence function is read in and its spectrum computed, or the coherence spectrum is read in. In either case, losses in signal gain are computed.

If LCOH > 0, the spatial-coherence function is read from unit LCOH and its spectrum computed. If, also, KCOH > 0, the spectrum is written onto unit KCOH.

If LCOH < 0, the coherence spectrum is read from unit KCOH (must be positive).

*Case 3*

KBEAM = 3: No losses in signal gain are computed. The NRL coherence model is evaluated and the computation of its spectrum is optional.

If LCOH > 0, the evaluated spatial-coherence function is written onto unit LCOH.

If KCOH > 0, the coherence spectrum is computed and written onto unit KCOH.

If KCOH = 0, the coherence spectrum is not computed.

If KCOH < 0, the coherence spectrum is computed but not written to an output file.

**Signal-Coherence Subroutines**

There are three subroutines concerned with computing signal coherence: MEDIUM, SPACOH, and WAVCOH.

*Subroutine MEDIUM*

This subroutine determines the parameters  $E$ ,  $k$ , and  $x$  of the NRL coherence model. Subroutine MEDIUM is activated only if the evaluation of the signal spatial-coherence function is requested. In subroutine MEDIUM, the variables

R, VL, CV, DRT, A, and E

are read in a card-image format, where

- $R = x$  = range to source (km),  
 $VL = l_v$  = vertical correlation length (m),  
 $CV = \bar{c}$  = average sound speed along signal path of propagation (m/s),  
 $DRT = \frac{\partial \bar{c}}{\partial T}$  = average partial derivative of sound speed with respect to temperature along signal path [(m/s)/°C],  
 $A = A_T^2$  = strength of temperature field (°C<sup>2</sup>/m), and  
 $E$  = the corresponding environmental factor.

If  $E$  is input as zero, it is computed from values of  $VL$ ,  $CV$ ,  $DRT$ , and  $A$ . If, in this case, any of the three parameters  $CV$ ,  $DRT$ , or  $A$  are input as zero, those equated to zero are determined from NP (input variable) profile sets. Each profile set is located at some range,  $RAN$ , and consists of one or more of four profiles: sound speed ( $C$ ), temperature ( $T$ ), Brunt-Väisälä frequency ( $BV$ ), and salinity ( $SALT$ ) (‰) versus depth ( $D$ ). For each of the NP ranges ( $RAN$ ), a profile set is input by reading NC card-image lines of the form

$$D(I), C(I), T(I), BV(I), SALT(I),$$

where NC is the number of depth points and

- $D(I)$  =  $i^{\text{th}}$  depth point (m),  
 $C(I)$  = sound speed at  $D(I)$  (m/s),  
 $T(I)$  = temperature at  $D(I)$  (°C),  
 $BV(I)$  = Brunt-Väisälä frequency  $\times 10^3$  at  $D(I)$  ( $10^{-3}$  rad/s),  
 $SALT(I)$  = salinity at  $D(I)$  (‰)

In all cases, a sound-speed profile [ $D(I)$  and  $C(I)$  values] must be specified or computed for depth-averaging purposes (see below). However, unless  $CV$  is input as zero, the  $C(I)$  values are not used to determine  $CV$ . The required sound speeds  $C(I)$  may either be specified or, if input as zero, be computed from Wilson's equation [32], corresponding input temperature  $T(I)$  and salinity  $SALT(I)$  values, and a computed pressure value [33]. Zero salinity values are reset to 35.

If  $CV$  is input as zero, we determine the average sound speed by first averaging the  $C(I)$  values over depth at each range then averaging the individual depth averages over the ranges of the NP sound-speed profiles.

If  $DRT$  is input as zero, a depth-range average temperature  $T$  is similarly found. The derivative  $DRT = \partial \bar{c} / \partial T$  is found from Wilson's equation, i.e.,

$$DRT = 4.623 - 0.1092T. \quad (31)$$

If  $A$  is input as zero, a depth-range average Brunt-Väisälä frequency ( $\times 10^3$ )  $BV$  is similarly found and the field strength  $A$  is found from [4]

$$A = BV \times 10^{-7}. \quad (32)$$

Similarly to the treatment of sound-speed profiles, if the  $BV(I)$  values of any profile set are input as zeroes (and  $A$  is input as zero), they are computed from corresponding input sound speed  $C(I)$ , temperature  $T(I)$ , salinity  $SALT(I)$ , and computed density values [33].

The depth averaging, performed at each range, is an approximation to averaging over the cyclic path of a dominant, horizontal signal arrival. A receiver depth, RD, is specified for which the sound speed is determined from the input sound-speed profile [i.e.,  $C(I)$  values — recall that  $C(I)$  must be specified]. Next, a reciprocal depth is found. If a true reciprocal depth does not exist, the reciprocal depth is taken to be either the ocean surface or the ocean bottom, whichever is appropriate. The reciprocal depth is assumed to be opposite in depth from the minimum sound speed (duct axis). That is, if the receiver depth is above the depth of the minimum sound speed (duct axis), the reciprocal depth is assumed to be below the duct axis, and vice versa.

The depth averaging described above assumes a horizontal arrival. To account for a dominant arrival that does not arrive horizontally, the receiver depth RD need only be reinterpreted as a depth where the dominant ray path becomes horizontal (vertex depth).

The foregoing discussions assumed that the environmental parameter E is input as zero, and also that at least one of the parameters CV, DRT, and A is input as zero. If a positive value is input for E, then VL, DRT, and A are ignored. However, a value for CV is required to convert from frequency to wavenumber. If zero is input for CV, its value is determined from input profile sets in an identical manner as in the case when E is input as zero.

#### *Subroutine SPACOH*

This subroutine evaluates the NRL coherence model using the environmental parameters determined by subroutine MEDIUM. Subroutine SPACOH evaluates the function

$$C(s) = \exp[-Ek_0^{5/2}xs^{3/2}] \quad (33)$$

at 4000 equally spaced samples of the separation distance  $s$ , between  $s = 0$  and  $s_M$ , where

$$C(s_M) = \exp(-32) = 1.26 \times 10^{-14}. \quad (34)$$

The value  $\exp(-32)$  was chosen to reduce the truncation error in approximating the infinite Fourier transform of  $C(s)$  by a finite transform. The large number of spatial samples reduces the aliasing effects of approximating a continuous transform by a discrete transform.

A subset of the sampled coherence function is printed. As an option, a CALCOMP plot of the spatial-coherence function is generated. Also, as an option, the sample values are written onto an output file on unit LCOH. This file may be used as an input file for later reruns of program COHORT.

#### *Subroutine WAVCOH*

This subroutine estimates the signal (coherence) spectrum by evaluating the discrete Fourier transform of sampled values of the spatial-coherence function. These sample values are either those found in subroutine SPACOH or comparable values read from an input file.

The signal spectrum  $S(k)$  is evaluated at  $k = 0$  and at symmetrical, equally-spaced samples spanning the domain  $-k_0 < k < k_0$ . The sample spacing in  $k$ -space is

$$\Delta_s = \frac{1}{N_f} \left( k_0 \frac{\lambda}{Nd} \right) = \frac{1}{N_f} (\Delta), \quad (35)$$

where  $\Delta$  is the separation in  $k$ -space of independent beams of an uniformly weighted line array with  $N$  elements equally spaced a distance  $d$  apart. It also corresponds to the distance between pattern nulls of such an array. The parameter  $N_f$  (called a fill factor) allows for a finer sampling than  $\Delta$ . Sample spacing is discussed further in the next subsection, which describes the array-performance subroutines.

The sample spacing  $\Delta_s$  is determined from the input parameters

$$\text{NPGS, NFILL, DISTPG, SS,}$$

where

$$\begin{aligned} \text{NPGS} &= N = \text{number of array elements, or group modules;} \\ \text{DISTPG} &= d = \text{distance (m) between array elements or group centers;} \\ \text{SS} &= c = \text{sound-speed (m/s) at the array; and} \\ \text{NFILL} &= N_f = \text{fill factor.} \end{aligned}$$

The total number of samples must not exceed 4000.

The signal spectrum is normalized by  $S(0)$  and referred to as the *field pattern*. Sample values of the field pattern are printed. As options, the field pattern can be plotted and/or written to an output file on unit KCOH.

If a comparable signal spectrum was computed by a previous computer run and written to an output file, that file can be read by subroutine WAVCOH, as an option, and the spectrum printed and, optionally, plotted. This option is an alternative to computing the spectrum from either input samples of the spatial coherence function or from one computed from input environmental parameters.

#### Array-Performance Subroutines

Array performance can be predicted for any of several array configurations. The receiver is assumed to be an array of identical hydrophone groups. A hydrophone group may consist of a single omnidirectional hydrophone, or it may be in itself a linear array of equally spaced hydrophones which cannot be steered from broadside. Nominally, the receiver is assumed to be a horizontal line array of  $N$  identical hydrophone groups equally spaced a distance  $d$  apart. The performance of other array configurations (e.g., distorted line array, nonequal spacing) can be predicted by the careful specification of  $N$  and  $d$  (to determine sample spacings and number of beams, see below) and by reading in the array pattern. In all cases, the receiver pattern is the *product pattern* of the *array pattern* times the *group pattern*, as shown in the section "Beam Patterns."

The field pattern (signal spectrum) computed in subroutine WAVCOH serves as an input to the array-performance subroutines. The beam patterns and the field pattern must be specified at the same sampled  $k$  values:  $k = 0$  and symmetrical, equally spaced values spanning  $-k_0 < k < k_0$ . The sample spacing is given by

$$\Delta_s = \frac{1}{N_f} k_0 \frac{\lambda}{Nd} = \frac{1}{N_f} \Delta, \quad (36)$$

which is determined in subroutine WAVCOH from input parameters. The distance  $\Delta$  is the spacing in  $k$ -space of the independent beams of a uniformly weighted line array of equally spaced elements. The output from  $N$  such beams is produced by the application of a discrete Fourier transform to element data (this is called FFT beamforming). For the broadside beam pattern of such an array, the spacing would produce pattern samples only at the main-beam axis and at nulls. The fill factor  $N_f$  is used to produce a finer sampling. There are two subroutines concerned with array performance prediction: BEAMS and CONVLV.

#### Subroutine BEAMS

This subroutine computes, prints, and, optionally, plots the array and group patterns. The input parameters of subroutine BEAMS are

## NPAT, NPFILL, NPH, and DISTPH.

The array pattern,  $B_a(k)$ , may either be read from card-image data or be computed. If the input parameter NPAT < 0, the parameter NPFILL is ignored and the array pattern is computed from

$$B_a(k) = B_a(k_0 \sin \theta) = \left[ \frac{\sin (Nkd/2)}{N \sin (kd/2)} \right]^2, \quad (37)$$

which is the theoretical pattern for a perfectly linear array of equally spaced hydrophones.

If the input parameter NPAT > 0, the parameter NPFILL is required to be identical to NFILL ( $N_f$ ) as a safety check, and the array pattern is input from card-image data in the following manner:

- NPAT values of the array pattern are read.
- Pattern values are read in order of increasing angles whose sines are integer multiples of

$$\frac{\Delta_s}{k_0} = \frac{1}{N_f} \left[ \frac{\lambda}{Nd} \right].$$

- The NCENth sample corresponds to  $\theta = 0$ , where NCEN = NPAT/2 if NPAT is even and NCEN = (NPAT + 1)/2 if NPAT is odd.

If the input array pattern does not span  $-\pi/2$  to  $+\pi/2$ , it will be repeated (in  $k$ -space) in order that the array pattern will be specified at the same sample points as the field pattern. Note that the pattern is strictly repeated. For example, if the first and last (NPAT) pattern values are zero (nulls), then two successive zero values will be generated whenever the pattern is repeated.

The group pattern,  $B_g(k)$ , is computed from

$$B_g(k) = \left[ \frac{\sin (Mkd_e/2)}{M \sin (kd_e/2)} \right]^2, \quad (38)$$

where

$M = NPH =$  number of hydrophones per group, and

$d_e = DISTPH =$  group hydrophone separation (m).

*Subroutine CONVLV*

Subroutine CONVLV convolves the field pattern (signal spectrum) with the array-group product pattern of the receiver to calculate the loss of signal gain (re ideal) for each of  $N$  beam directions. The  $N$  beam directions, or angles, bracket the signal direction and are spaced at intervals of

$$\Delta = k_0 \frac{\lambda}{Nd} \quad (39)$$

in  $k$  space. The  $N$  beams are numbered sequentially from negative to positive such that the main axis of beam number 0 coincides with the signal direction. The convolution can be performed for several signal directions.

The input parameters of subroutine CONVLV are

NSHF (I), I = 1, NCENT,

which specify NCENT signal-arrival directions, for each of which the field and product patterns are convolved. For each signal case, the signal-arrival angle corresponds to the main-axis angle of the beam whose beam number is given by NSHF(I), i.e.,

$$\sin\theta_s = \text{NSHF}(I) \cdot \frac{\lambda}{Nd}, \quad (40a)$$

or in wavenumber space,

$$k_s = \text{NSHF}(I) \cdot \frac{k_0\lambda}{Nd}. \quad (40b)$$

For each signal case, the (signal) field pattern is also shifted from broadside to the arrival direction  $k_s$ , as shown in Fig. 7. The receiver pattern is steered sequentially through the  $N$  beam angles bracketing the signal direction. For each steering, the shifted field and product patterns are multiplied and scaled to estimate the loss in signal gain for that beam. This process is repeated for subsequent signal arrival directions if  $\text{NCENT} > 1$ .

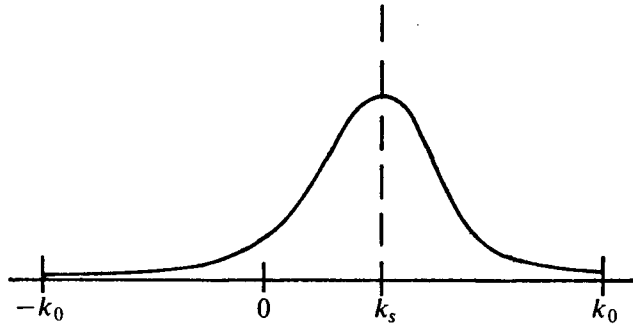


Fig. 7 — Field pattern for arrival direction  $k_s$

Recall that only the array pattern and not the group pattern can be steered, and that the product pattern is normalized by the group-pattern response in the steered direction (to maintain a constant main-axis response). For example, when the array is steered to the direction  $k_r$ , the receiver product pattern is

$$B_p(k, k_r) = B_a(k - k_r)B_g(k)/B_g(k_r), \quad (41a)$$

or

$$B_p(k_r, k_r) = B_a(0). \quad (41b)$$

For each signal-arrival direction  $k_s$ , subroutine CONVLV prints the parameters

- $\theta_i$  = beam angle (re signal arrival-angle),
- $L(k_i, k_s)$  = loss of signal gain (re ideal),
- $B_g(k_i)$  = product pattern normalization,
- $B_a(0)$  = main-axis response of array pattern, and
- $S(k_i - k_s)$  = signal-field strength at beam angle  $\theta_i$

as functions of beam number  $i$ . Also, as an option, a plot of loss versus (relative) beam-angle is generated.

After all NCENT signal cases are processed, the losses at each (relative) beam-angle are averaged (over the signal cases or array shifts). These averages are printed and, optionally, plotted.

## OPERATING INSTRUCTIONS

This section describes the card-image input-data structure of program COHORT and presents a sample set of JSL instructions for executing the program on the ASC resident at NRL.

### Card-Image Input

This section begins with a card-by-card description of the COHORT card-image input data followed by a summary of this structure. Next is a table of the input structures for the three basic options of program COHORT. A flowchart outlining the various program options and a sample set of JSL instructions conclude the section.

#### Card-Image Data

The following describes the input-data structure for running program COHORT:

Card 1 inputs are KBEAM, LCOH, KCOH, AND KPLOT, with format (4I5), where

KBEAM = code for selecting program options,  
 LCOH = logical unit for reading or writing spatial coherence,  
 KCOH = logical unit for reading or writing coherence spectrum, and  
 KPLOT specifies options for plotting coherence.

Options are as follows:

- KBEAM = 1, compute spatial coherence and determine beam outputs,
  - LCOH > 0, write spatial coherence onto unit LCOH;
  - KCOH > 0, write coherence spectrum onto unit KCOH;
- KBEAM = 2, input coherence and determine beam outputs,
  - LCOH > 0, read spatial coherence from unit LCOH and compute coherence spectrum; if also KCOH > 0, write spectrum onto unit KCOH;
  - LCOH ≤ 0, read coherence spectrum from unit KCOH (must be positive);
- KBEAM = 3, compute coherence only,
  - LCOH > 0, write spatial coherence onto unit LCOH;
  - KCOH < 0, compute spectrum, but do not write to an output file;
  - KCOH = 0, do not compute spectrum;
  - KCOH > 0, compute spectrum and write onto unit KCOH;
- KPLOT = 0, do not generate plots of coherence;
- KPLOT = 1, plot only spatial coherence;
- KPLOT = 2, plot both spatial coherence and its spectrum;
- KPLOT = 3, plot only spectrum.

Card 2 input is F, with format (F10.2), where

F = acoustic frequency (Hz).

Card 3 inputs are R, VL, CV, DRT, A, and E, with format (4F10.2, 2E10.2).

These parameters specify the NRL coherence model, where

R = range (km),  
 VL = vertical correlation length (m),  
 CV = average sound speed (m/s),  
 DRT = average partial derivative of sound speed with respect to temperature [(m/s)/°C],  
 A = strength of temperature fluctuations (°C<sup>2</sup>/m), and  
 E = corresponding environmental parameter.

NOTE: This card is read only if KBEAM = 1 or 3 (coherence functions are read in rather than computed when KBEAM = 2).

Card 4a inputs are NP and RD, with format (I5, F10.2), where

NP = number of profile sets to follow, and  
 RD = receiver depth (m).

Card 4b inputs are NC, RAN, and FLAT, with format (I5, 2F10.2), where

NC = number of depth points to follow,  
 RAN = range of profile set (km), and  
 FLAT = latitude of profile set (deg)—ignored unless sound speeds are calculated.

Card 4c inputs are (D(I), S(I), T(I), BV(I), SALT(I), I = 1, NC), with format (5F10.2,/), where

D(I) = Ith depth (m),  
 S(I) = Ith sound-speed (m/s),  
 T(I) = Ith temperature (°C),  
 BV(I) = Ith Brunt-Väisälä frequency ( $r/s \times 10^3$ ), and  
 SALT(I) = Ith salinity (‰)—defaults to 35.

NOTE: One Card 4b followed by NC Cards 4c are read for each of NP ranges.

Cards 4a through 4c are read only if KBEAM = 1 or 3 if E = 0 and any one of CV, DRT, and A is zero or if E > 0 and CV = 0.

See the section on Subroutine MEDIUM for a complete description of options for specifying parameters of the coherence model.

Card 5 inputs are NGPS, NFILL, DISTPG, and SS, with format (2I5, 2F10.5), where

NGPS = number of group modules,  
 NFILL = fill factor for evaluating coherence spectrum,  
 DISTPG = distance between center points of any two adjacent group modules (m), and  
 SS = sound speed at the array (m/s).

NOTE: Sample coherence-spectrum values are equally spaced in  $k$  space by

$$\Delta_s = \frac{k_0^*SS/F}{NFILL*NGPS*DISTPG} = \frac{k_0\lambda}{N_fNd} = \frac{1}{N_f}\Delta.$$

This card is read only if

- (iii) KBEAM = 1 (spatial coherence and spectrum computed), or
- (iii) KBEAM = 2 and LCOH > 0 (spatial coherence input and spectrum computed), or
- (iii) KBEAM = 3 and KCOH  $\neq$  0 (spatial coherence and spectrum computed).

If KBEAM = 3, no more cards follow.

Card 6 inputs are KBMPLT, NPAT, NPFILL, NPH, NCENT, and DISTPH, with format (5I5, F10.2), where

- KBMPLT > 0, plot group and array patterns;
- NPAT > 0, read in number of array-pattern values;
- NPAT < 0, compute standard array pattern;
- NPFILL = fill factor of sample beam-pattern values; ignore if NPAT < 0; if NPAT > 0, NPFILL must equal NFILL, which is checked for; normally, NPAT = NGPS\*NPFILL;
- NPH = number of hydrophones per group module;
- NCENT = number of beam shifts desired (0 < NCENT < 9); and
- DISTPH = distance between individual group phones (m).

Card 7 inputs are (NSHF(I), I = 1, NCENT), with format (16I5), where

NSHF(I) = amount of shift of Ith beam shift in units of the spacing of the independent array-pattern beams in  $k$  space; this spacing is given by

$$\Delta = \frac{k_0^*SS/F}{NGPS*DISTPG} = \frac{k_0\lambda}{Nd}.$$

Card 8 input are (PAT(I), I=1, NPAT), with format (8E10.2), where

PAT(I) = array pattern in real units (i.e., not dB).

NOTE: Array pattern values must be equally spaced in  $k$  space by  $\Delta_s$ .

This card is read only if NPAT > 0.

Card 9 input is KASPLT, with format (I5), where

- KASPLT specifies options for plotting signal loss;
- KASPLT = 0, no plots generated;
- KASPLT = 1, plot array signal loss for each of NCENT signal cases;
- KASPLT = 2, plot loss for each case and average loss for all cases; and
- KASPLT = 3, plot average signal loss for totality of losses.

The following is a summary of the card-image data read by program COHORT:

Card	Inputs	Format
1	KBEAM, LCOH, KCOH, KPLOT	(4I5)
2	F	(F10.2)
3	R, VL, CV, DRT, A, E	(4F10.2, 2E10.2)
4a	NP, RD	(I5, F10.2)
4b	NC, RAN, FLAT	(I5, 2F10.2)
4c	D(I), S(I), T(I), BV(I), SALT(I) (repeat NC times)	(5F10.2,/)
	} repeat NP times	
5	NPGPS, NFILL, DISTPG, SS	(2I5, 2F10.5)
6	KBMPLT, NPAT, NPFILL, NPH, NCENT, DISTPH	(5I5, F10.2)
7	(NSHF(I), I = 1, NCENT)	(16I5)
8	(PAT(I), I = 1, NPAT) (repeat NPAT/8 times)	(8E10.2)
9	KASPLT	(I5)

The following is a table listing the required and optional input-data cards for the program options determined by the input value of KBEAM.

*Option Table*

The following table shows the input structures for the three basic options of program COHORT:

Card	KBEAM = 1		KBEAM = 2		KBEAM = 3		Subroutine
	Required	Optional	Required	Optional	Required	Optional	
1	X		X		X		—
2	X		X		X		—
3	X				X		MEDIUM
4a		X				X	MEDIUM
4b		X				X	MEDIUM
4c		X				X	MEDIUM
5	X			X		X	WAVCOH
6	X		X				BEAMS
7	X		X				CONVLV
8		X		X			BEAMS
9	X		X				—

*Flowchart*

The following flowchart, Fig. 8, relates the card-image data with the program options prescribed by the parameters KBEAM, LCOH, and KCOH.

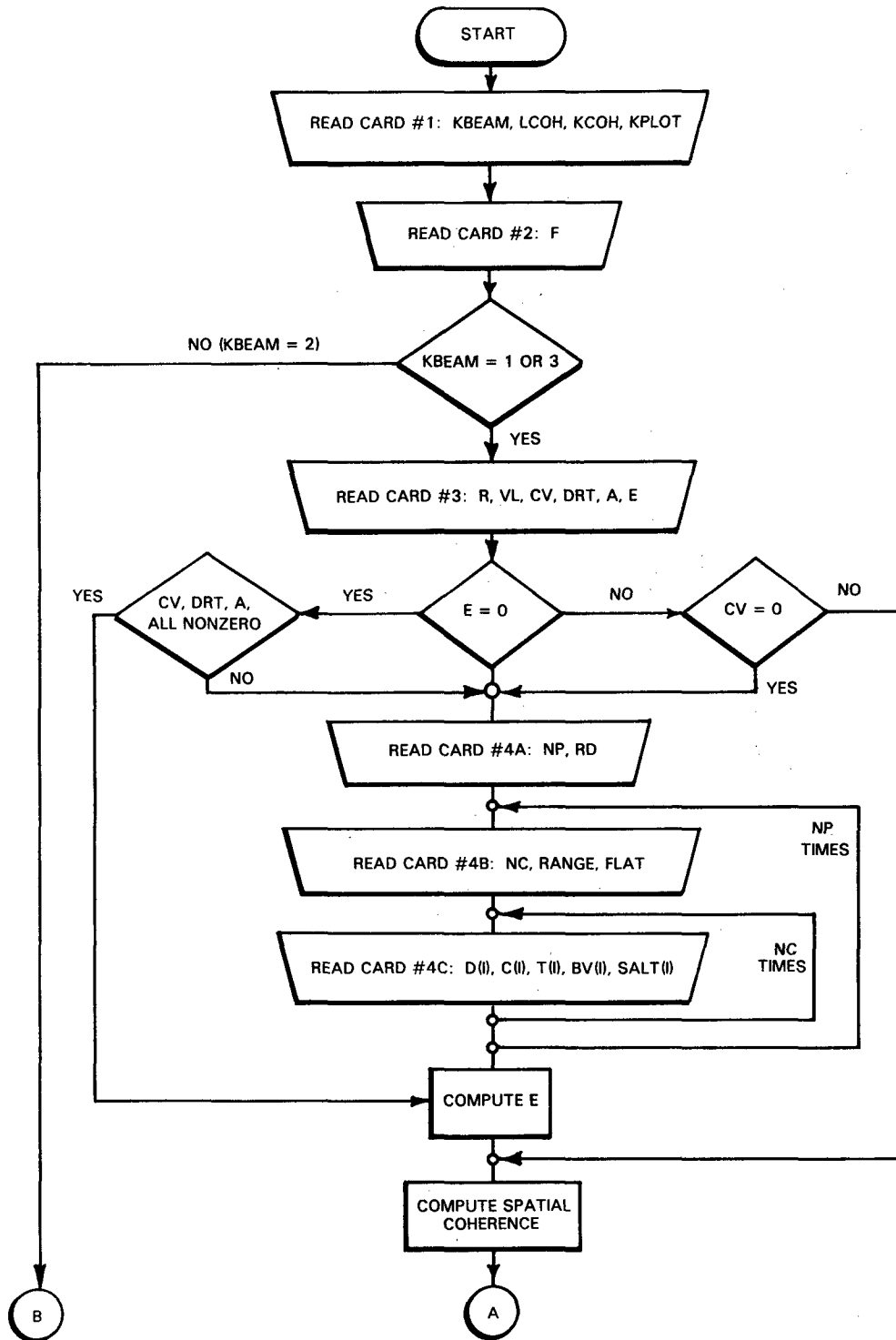


Fig. 8 - Flowchart for COHORT

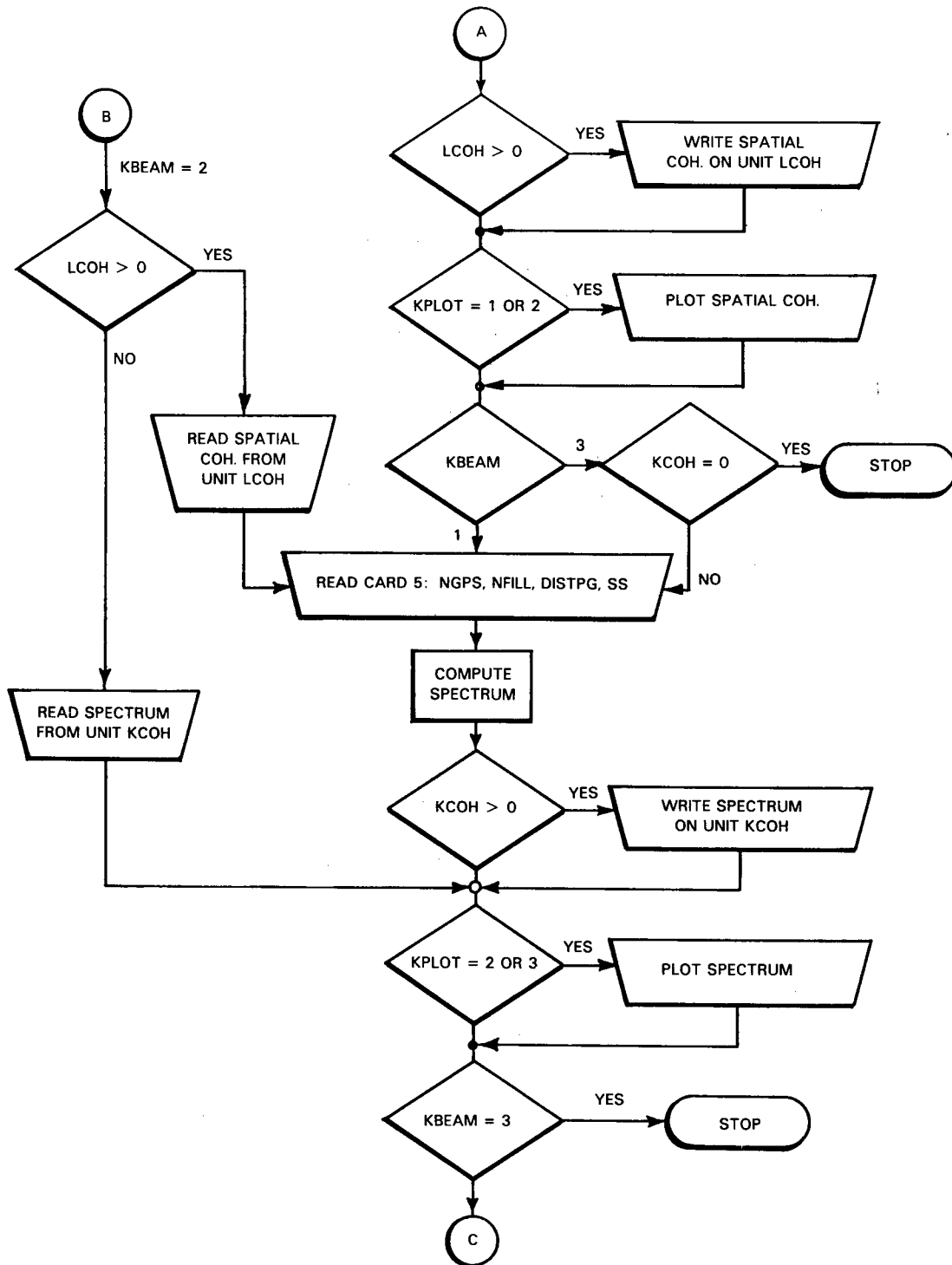


Fig. 8 (Continued) - Flowchart for COHORT

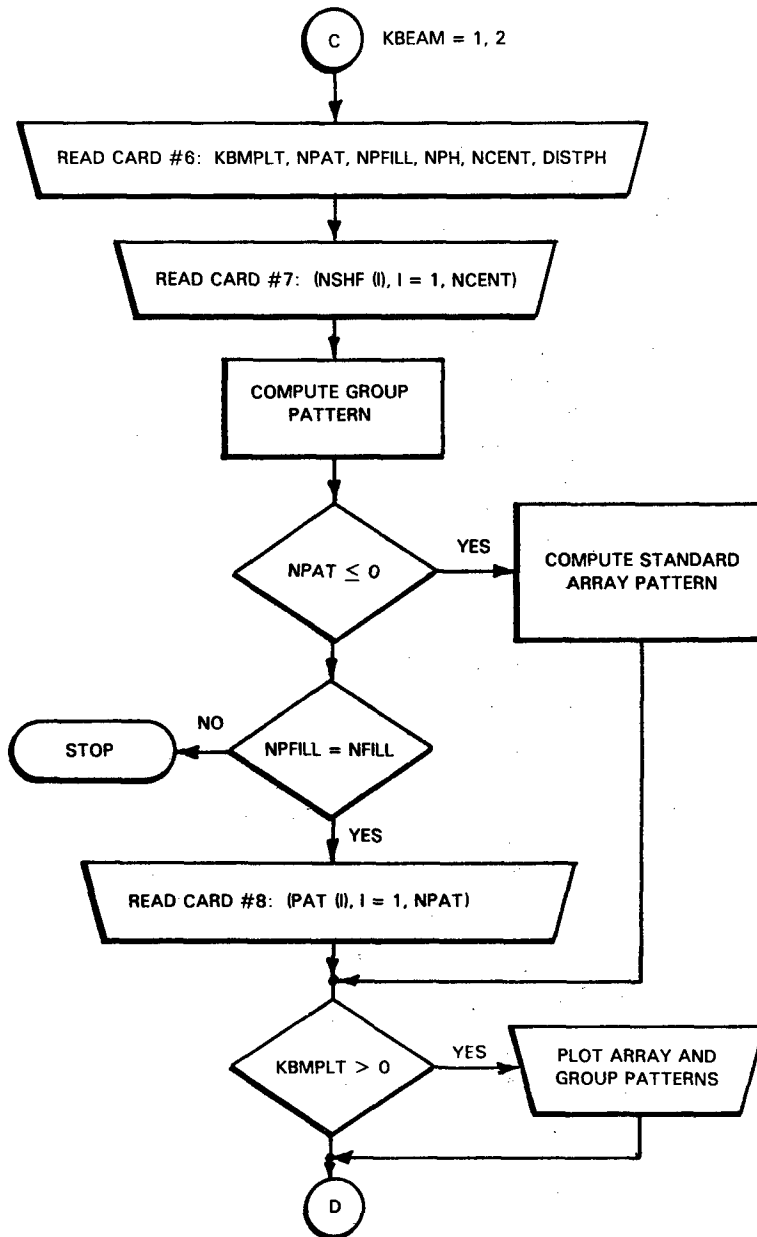


Fig. 8 (Continued) — Flowchart for COHORT

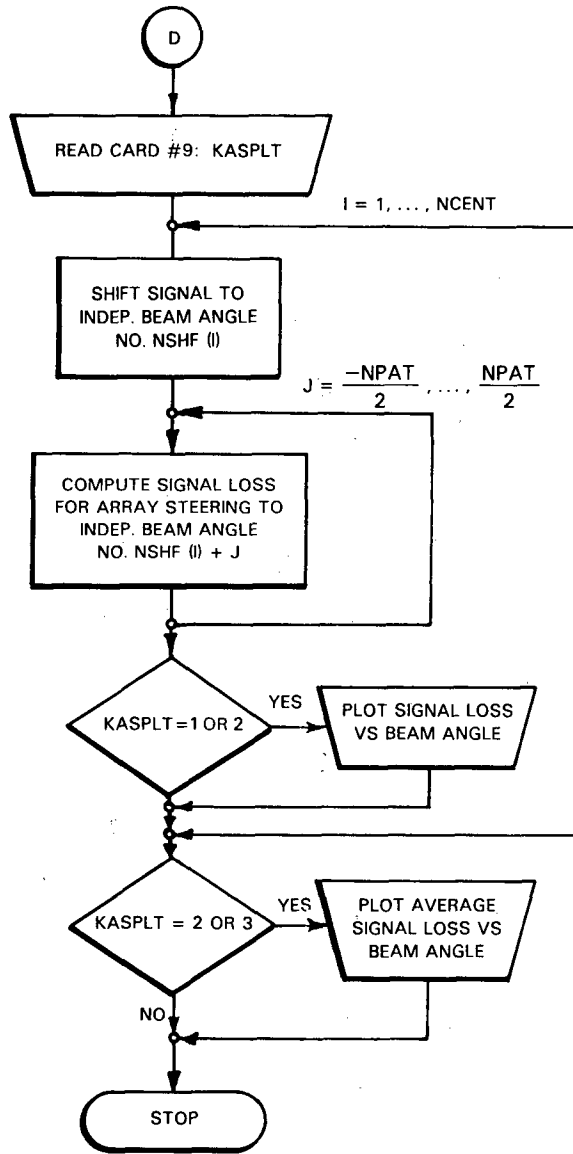


Fig. 8 (Continued) — Flowchart for COHORT

**Sample JSL Commands**

The following is a sample set of JSL instructions for executing COHORT on the ASC system:

```

/ JOB, jobname, account number, usercode, CAT = 1, OPT = (T, R)
/ LIMIT BAND = 50, SEC = 120
/ JSLOPTS OPT = (F, L, M)
/ PD YOU, USERCAT/D-/B-/usercode/node
/ ASG SYS.OMOD, USERCAT/D81/L60/COHORT/OBJECT, USE = SHR
/ ASG FT01F001, YOU/SCOH, USE = SHR*
/ ASG FT02F001, YOU/KSPEC, USE = SHR*
/ FD FT06F001, BAND = 2/20/2
/ LNK
/ FXQT CPTIME = 10000
...
card-image data
...

/ FOSYS FT06F001
/ CAT YOU/SCOH, ACNM = FT01F001†
/ CAT YOU/KSPEC, ACNM = FT02F001†
/ FOSYS FT59F001, TYPE=PLOT, FORM=00‡
/ EOJ

```

---

\*††The inclusion of these commands depends upon user-selectable options.

\*If it is specified that an input file is to read from logical unit *N*, then a JSL command of the form  
/ ASG FTONF001, YOU/FILENAME, USE=SHR

must be supplied.

†If it is specified that an output file is to be written onto logical unit *N*, then a JSL command of the form  
/ CAT YOU/FILENAME, ACNM = FTONF001

must be specified.

‡If one or more CALCOMP plots are requested, then this JSL command must be furnished.

## REFERENCES

1. J.J. McCoy and J.S. Perkins, "Transverse Vertical Coherence of a Macroray Path Induced by an Inhomogeneous Anisotropic Ocean," in preparation.
2. J.S. Perkins, R.N. Baer, L.F. Roche, and L.B. Palmer, "Three-Dimensional Parabolic-Equation-Based Estimation of the Ocean Acoustic Field," NRL Report 8685, Mar. 31, 1983.
3. R.N. Baer, J.S. Perkins, E.B. Wright, and J.J. McCoy, "Stochastic Propagation of the Mutual Coherence Function in the Deep Ocean," in preparation.
4. W.B. Moseley and L.B. Palmer, "Ocean Basin Transverse Horizontal Coherence Limits and Array Design," in preparation.
5. F.D. Tappert, in *Wave Propagation and Underwater Acoustics*, edited by J.B. Keller and J.S. Papadakis, Springer-Verlag, New York, 1977, pp. 224-287.
6. P.G. Bergmann, *Phys. Rev.* **70**, 486 (1946).
7. D. Mintzer, *J. Acoust. Soc. Am.* **25**, 922 (1953).
8. C.L. Pekeris, *Phys. Rev.* **71**, 268 (1942).
9. L.A. Chernov, *Wave Propagation in a Random Medium*, translated by R.A. Silverman, McGraw-Hill, New York, 1960.
10. V.I. Tatarski, *Wave Propagation in a Turbulent Medium*, translated by R.A. Silverman, McGraw-Hill, New York, 1961.
11. V.I. Tatarski, *The Effects of the Turbulent Atmosphere on Wave Propagation*, translated from Russian, National Technical Information Service, Springfield, Virginia, 1971.
12. W. Munk and F. Zachariassen, *J. Acoust. Soc. Am.* **59**, 818-838 (1976).
13. M.J. Beran and J.J. McCoy, *J. Math. Phys.* **15**, 1901-1912 (1974).
14. M.J. Beran and J.J. McCoy, *J. Acoust. Soc. Am.* **56**, 1667-1672 (1974).
15. M.J. Beran and J.J. McCoy, *J. Acoust. Soc. Am.* **17**, 1186-1189 (1976).
16. I.M. Besieris and F. Tappert, *J. Math. Phys.* **14**, 1829-1836 (1973).
17. I.M. Besieris and F. Tappert, *J. Math. Phys.* **17**, 734-743 (1976).
18. F.D. Tappert, *J. Opt. Soc. Am.* **66**, 1368-1373 (1976).
19. J.J. McCoy and M.J. Beran, *J. Acoust. Soc. Am.* **59**, 1142-1149 (1976).
20. J.J. McCoy and M.J. Beran, *J. Acoust. Soc. Am.* **65**, 1468-1481 (1979).

21. L.B. Wilson and F.D. Tappert, "Acoustic Propagation in Random Oceans Using the Transport Equation," Report SAI-78-639-LJ, Science Applications Incorporated, La Jolla, California, Apr. 1978.
22. R. Dashen, *J. Math. Phys.* **20**, 894-920 (1979).
23. G.R. Sutton and J.J. McCoy, *J. Acoust. Soc. Am.* **60**, 833-839 (1976).
24. G.R. Sutton and J.J. McCoy, *J. Math. Phys.* **18**, 1052-1057 (1977).
25. L.B. Dozier and F.D. Tappert, *J. Acoust. Soc. Am.* **63**, 353-365 (1978).
26. L.B. Dozier and F.D. Tappert, *J. Acoust. Soc. Am.* **64**, 533-547 (1978).
27. S.M. Flatté, *Sound Transmission Through a Fluctuating Ocean*, Cambridge Univ. Press, New York, 1979.
28. A.W. Ellinthorpe et al., Naval Underwater Systems Center Technical Memoranda associated with the Joint Oceanographic/Acoustic Experiment, 1975-1977.
29. T.E. Ewart, *J. Acoust. Soc. Am.* **60**, 46-59 (1976).
30. M.S. Beran, J.J. McCoy, and B.B. Adams, "Effects of a Fluctuating Temperature Field on the Spatial Coherence of Acoustic Signals," NRL Report 7809, 1975.
31. G.H. Robinson, *J. Acoust. Soc. Am.* **69**, 112-123 (1981).
32. W.D. Wilson, *J. Acoust. Soc. Am.* **32**, 641-644 (1960).
33. W.B. Moseley and D.R. DelBalzo, "Temperature Microstructure of the Ocean Near the Deep Sound Channel Axis," NRL Report 7729, 1974.

Appendix  
SAMPLE CASE

This appendix describes a sample execution of program COHORT. The purpose of this example is to provide a numerical illustration of the type of output program COHORT is capable of producing and to serve as a guide to the user initially attempting to execute the program. The option selected (KBEAM=1) computes both signal coherence and array performance, thus utilizing all the subroutines (or functions) of program COHORT.

**INPUT DATA**

The card-image input data used to generate the sample results are listed in Fig. A1.

1	0	0	2			
300						
2000.0	0	30.	1501.1	4.26		
1	0.					
44	0.	32.5				
0.00	1535.00	23.21	36.561			
20.81	1532.09	23.20	36.565			
23.39	1530.85	22.50	36.523			
25.97	1529.59	22.00	36.493			
28.55	1528.31	21.50	36.465			
31.78	1527.07	21.09	36.557			
35.51	1525.86	20.83	36.577			
39.24	1524.63	19.96	36.576			
46.37	1523.37	19.51	36.571			
58.25	1522.13	18.99	36.529			
63.75	1520.72	18.54	36.541			
68.43	1519.26	17.90	36.357			
76.66	1517.97	17.43	36.380			
131.85	1517.37	17.01	36.385			
217.83	1517.16	16.50	36.262			
243.96	1515.90	16.05	36.134			
266.35	1512.97	14.93	35.873			
284.17	1509.97	14.02	35.770			
314.63	1506.80	12.95	35.612			
346.14	1503.66	11.98	35.394			
410.93	1501.22	11.01	35.395			
472.75	1498.53	9.98	35.284			
534.36	1495.70	9.00	35.163			
620.29	1493.33	8.00	35.137			
706.59	1490.85	7.02	35.112			
815.93	1488.65	6.00	35.061			
851.45	1488.24	5.76	35.071			
894.91	1487.94	5.50	35.059			
971.13	1488.21	5.25	35.069			
1033.07	1488.20	5.00	35.050			
1150.72	1489.15	4.75	35.059			
1258.26	1489.88	4.51	35.035			
1359.42	1490.51	4.25	35.004			
1501.31	1491.82	4.00	34.980			
1683.38	1494.37	3.88	34.981			
1855.52	1496.76	3.75	34.978			
2063.63	1499.76	3.62	34.977			
2170.07	1501.04	3.50	34.967			
2295.27	1502.64	3.37	34.963			
2454.74	1504.83	3.25	34.955			
2599.43	1506.78	3.13	34.947			
2729.31	1509.47	3.00	34.940			
3800.00	1524.05	2.84	34.929			
4800.00	1541.76	2.84	34.929			
128	2	5.0	1500.0			
1	0	2	3	1.25		
0	5	10				

Fig. A1 — Card-image input data for sample case

## ENVIRONMENTAL PARAMETERS

To compute spatial coherence, the signal source was assumed to be located at a range of 2000 km and to transmit at an acoustic frequency of 300 Hz. To compute the environmental parameter

$$E = 1.7 \left[ \frac{1}{\bar{c}} \frac{\partial \bar{c}}{\partial T} \right]^2 l_V A_T^2,$$

it was assumed that

$$\bar{c} = 1501.1 \text{ (m/s),}$$

$$\frac{\partial \bar{c}}{\partial T} = 4.26 \text{ (m/s)/}^\circ\text{C,}$$

and

$$l_V = 30 \text{ m;}$$

but the strength of the random temperature fluctuations  $A_T^2$  was assumed to be unknown. To estimate  $A_T^2$  (which is, effectively, the average Brunt-Väisälä frequency along the propagation path) a single profile set was input. The profile set specified sound speed, temperature, and salinity at each of 44 depths. Recall that zero sound speeds are recalculated from temperature, depth, salinity, and latitude. The profile-set range was arbitrarily set to zero and the latitude taken to be  $32.5^\circ$  (ignored here).

The receiver depth was set at zero (the sea surface), which resulted in the Brunt-Väisälä frequency's being averaged between the sea surface and a depth of 4418 m (the reciprocal depth). The computed strength parameter was

$$A_T^2 = 1.48 \times 10^{-7},$$

which resulted in

$$E = 6.09 \times 10^{-11}.$$

## SIGNAL COHERENCE

Next, the normalized coherence function was evaluated as a function of horizontal separation. The optional plot of the normalized spatial coherence function is shown in Fig. A2. Finally, the option to compute and plot the wavenumber spectrum of signal coherence was exercised, and the result is shown as Fig. A3.

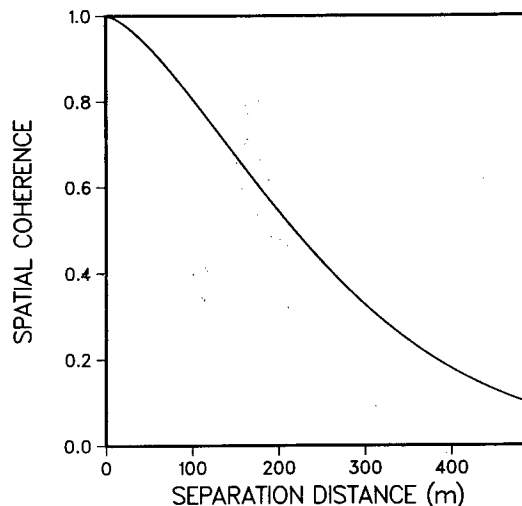
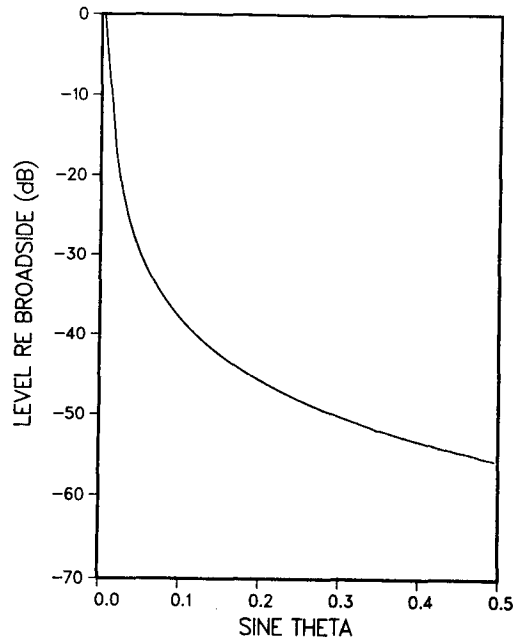


Fig. A2 — Normalized spatial coherence

Fig. A3 — Normalized wavenumber spectrum of signal coherence



### BEAM PATTERNS

The horizontal receiving array was assumed to consist of 128 hydrophone groups equally spaced 5 m apart (center-to-center). Each hydrophone group was assumed to consist of four omnidirectional hydrophones spread 1.25 m apart. Corresponding plots of the array and group beam-patterns are shown in Figs. A4 and A5, respectively.

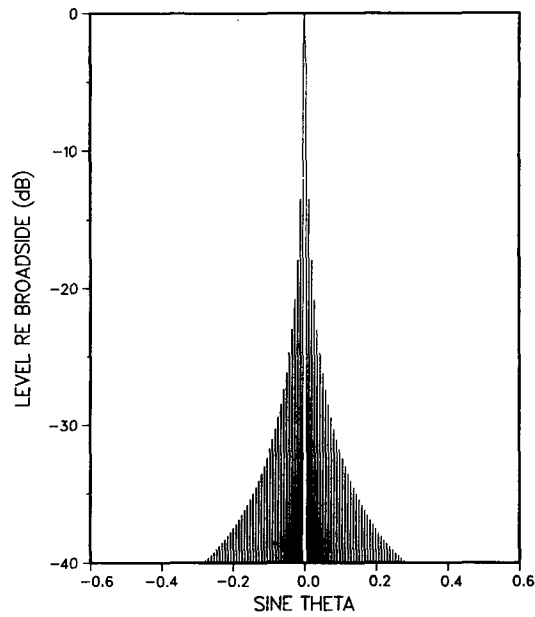


Fig. A4 — Array beam pattern

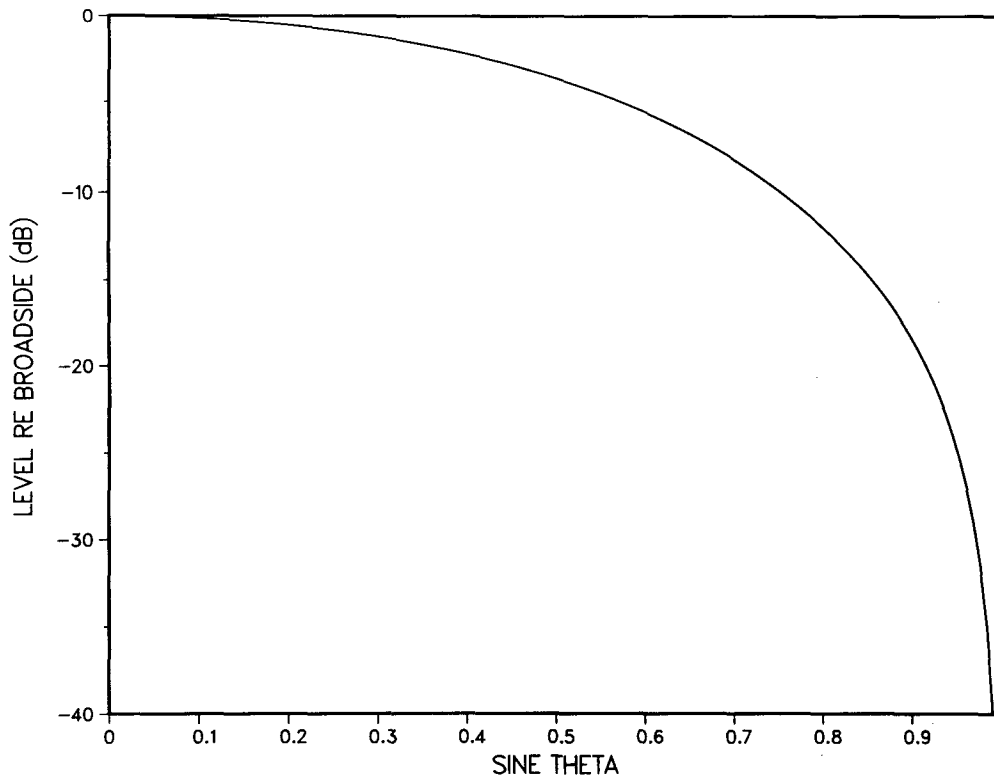


Fig. A5 — Group beam pattern

For the above array configuration, independent beams (and also nulls) are equally spaced in wavenumber space by

$$\Delta \approx 16\pi \times 10^{-4} \text{ m}^{-1}.$$

If the array were not more finely sampled, it would be specified at the main-beam axis (unit response) and at nulls (zero response). To affect a meaningful convolution, the sampling rate was increased by a factor of 2 (i.e., NFILL=2). Array, group, and signal patterns were sampled (internally) at this spacing.

## ARRAY PERFORMANCE

Array performance was predicted for each of three signal-arrival angles. As required, each arrival angle corresponded to the main-beam axis of an independent beam angle of the array pattern (with the  $0^\circ$  broadside beam angle serving as a reference). Recall that these beam angles are on the main-beam axes of spatially independent beams that would result if the array were perfectly linear (which in this case, it is) and the hydrophone groups each consisted of a single omnidirectional hydrophone. For the example considered of a 128-element array, there are 128 such beams, numbered here between  $-63$  and  $+64$  with beam 0 representing the broadside beam pattern.

The three signal-arrival angles selected correspond to independent beams 0 (broadside), 5, and 10. For each arrival angle, signal gain degradation was computed for each of 128 independent beams (directions), where now the reference beam number 0 is directed at the signal-arrival direction. Therefore, for each case the signal-gain degradation is computed for each of the 128 beam angles that would result from phase-steering the array to the signal direction and performing FFT beamforming.

The resulting plots of signal-gain degradation for the three signal directions are shown in Figs. A6 through A8. For reference, computed signal-gain degradations are given in Table A1.

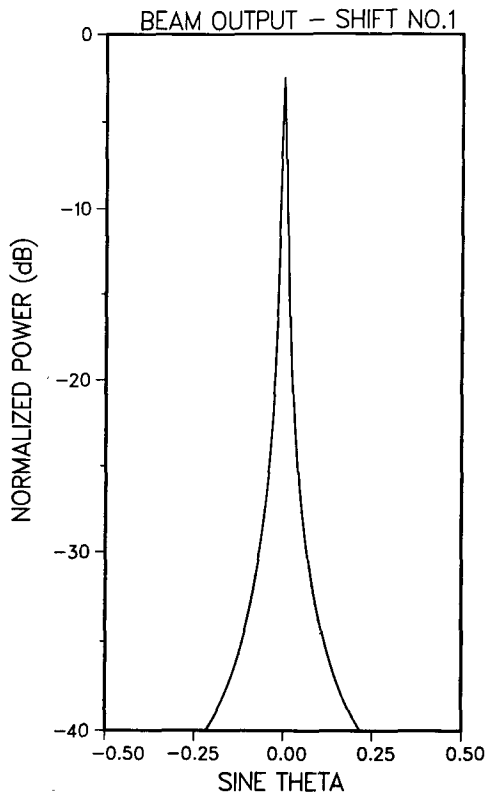


Fig. A6 - Normalized array signal gain for broadside signal arrival

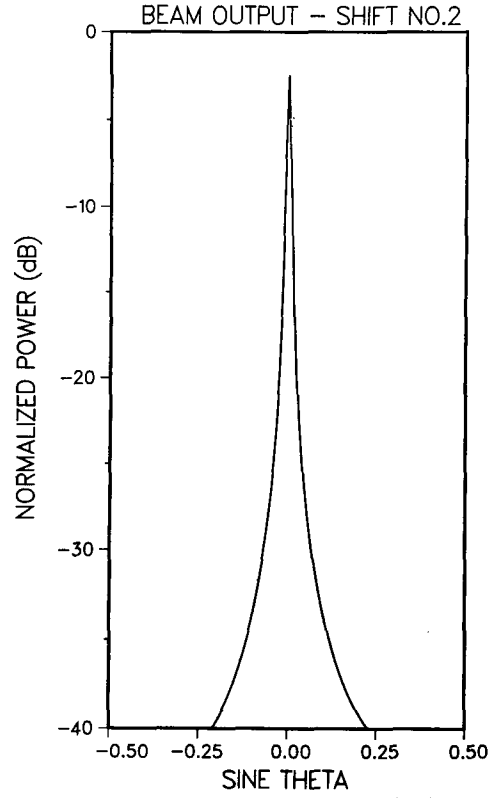


Fig. A7 - Normalized array signal gain for beam 5 arrival

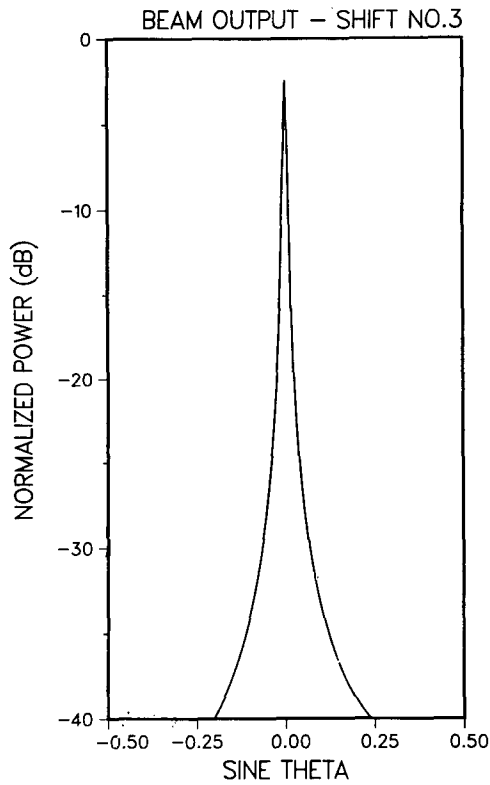


Fig. A8 - Normalized array signal gain for beam 10 arrival

Table A1—Signal-Gain Degradation

Receiver Beam	Signal-Gain Degradation (dB)		
	Signal Beam 0	Signal Beam 5	Signal Beam 10
0	2.49	2.49	2.49
8	29.36	29.27	29.18
16	35.65	35.48	35.31

Finally, signal-gain degradation for each beam is averaged over the signal-arrival cases. The result is plotted in Fig. A9.

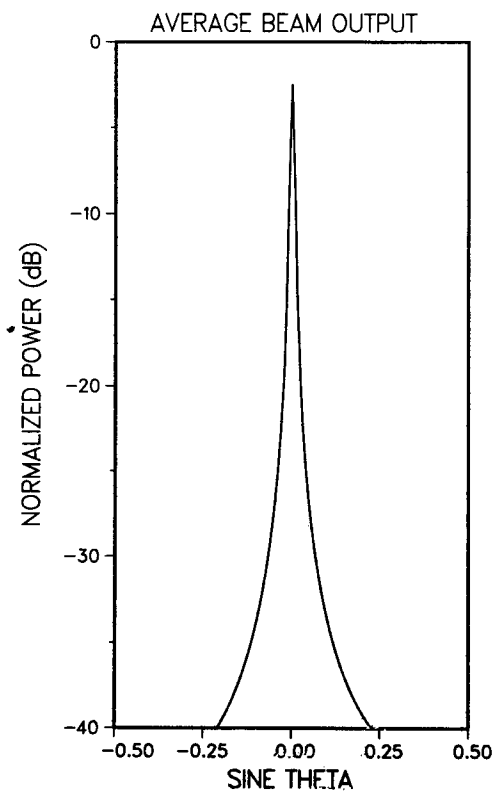


Fig. A9 — Average normalized array signal gain for the three signal-arrival cases